Group-theory approach to tailored electromagnetic properties of metamaterials: An inverse-problem solution

Charles M. Reinke, Teofilo M. De la Mata Luque, Mehmet F. Su, Michael B. Sinclair, and Ihab El-Kady

Phys. Rev. E **83**, 066603 — Published 16 June 2011

DOI: 10.1103/PhysRevE.83.066603

Group theory approach to tailored electromagnetic properties of metamaterials: an inverse problem solution

Charles M. Reinke[1], Teofilo M. De la Mata Luque[2], Mehmet F. Su[2], Michael B. Sinclair[1], and Ihab El-Kady [1,2†]

[1] Sandia National Laboratories, PO Box 5800, Albuquerque, NM 87123, U.S.A.
[2] 1 University of New Mexico, Albuquerque, NM 87131, U.S.A.

(Received: August 25, 2010)

ABSTRACT

The problem of designing electromagnetic metamaterials is complicated by the pseudo-infinite parameter space governing such materials. We present a general solution based on group theory for the design and optimization of the electromagnetic properties of metamaterials. Using this framework, the fundamental properties of a metamaterial design, such as anisotropy or magnetic or electrical resonances, can be elucidated based on the symmetry class into which the unit cell falls. This provides a methodology for the inverse problem of design of the electromagnetic properties of a metamaterial. We also present simulations of a Zia metamaterial that provides greater design flexibility for tuning the resonant properties of the device that a structure based on a simple split-ring resonator. The power of this Zia element is demonstrated by creating bianisotropic, chiral, and biaxial designs using the inverse group theory procedure outlined in this paper.

PACS Codes: 81.05.Xj (metamaterials), 02.20.-a (group theory), 81.05.Xj (bianisotropic media),

† Corresponding author: ielkady@sandia.gov

1. INTRODUCTION

During the last few years, metamaterials (MMs) have received significant attention in research due to their anomalous electromagnetic properties [1] and, hence, their potential for unique applications. In 1968, Veselago proposed the a particular class of MMs, referred to as a left-handed metamaterial (LHM), which had several unusual properties, phase and energy flux of opposing sign, a negative index of refraction, reversal of the Doppler effect, and flat lens focusing [2]. More generally, a MM is any artificial material that exhibits electromagnetic properties that are not necessarily displayed by the constituent elements. This is primarily due to resonant effects arising from the periodic orientation of the individual elements, which are typically sub-wavelength in size. Thus, electromagnetic MMs can theoretically exhibit any value of permittivity or permeability near the resonance frequency, including negative values. This prospect has led to the proposal of applications ranging from superlenses [3] and the enhancement of antenna systems [4], to arguably even electromagnetic cloaking [5].

Despite the growing body of work involving MMs, little consensus has emerged regarding the optimal structure for producing a given set of electromagnetic properties, although a few general design templates such as the split-ring resonator (SRR) [6] have become popular, largely due to their relative ease of fabrication. However, the number of different element designs that have been published almost rivals the number of groups investigating MMs. The variety of designs is a reflection of the lack of a formalized method for designing such structures. Thus, MM design is often a cyclic process of "educated guesswork" and trial-and-error, making extensive use of numerical simulations that are occasionally combined with optimization techniques such as genetic algorithms.

The problem of designing electromagnetic MM is complicated by the pseudo-infinite parameter space governing such materials. If we consider a MM unit cell composed of a simple circular SRR on the six faces of a cube, there are $4^6 = 4096$ possible orientations of the cell in the

most general case. Even if we eliminate the orientations that are indistinguishable due to symmetry and invoke the quasi-static limit, the number of possibilities that would have to be tried in a brute-force approach only reduces to 128. Given typical simulation times the order of tens of hours for a fully-vectorial numerical electromagnetic simulation for this type of structure, the problem quickly becomes intractable. Additionally, such simulations only provide the net result with limited insight into the inter-element interactions.

In this paper, we present general approach to the inverse problem solution based on group theory for the design and optimization of the electromagnetic properties of MMs. There have been prior attempts at using group theory analysis for understanding MM behavior and inferring design such as the seminal work by Padilla [7] and a subsequently demonstration by Wongkasem, *et al*. [8]. These papers, however, lack the systematic inverse design route that is outlined here, and additionally assume erroneous interpretations of the character table and the coupling of the linear and axial modes that would make it virtually impossible to design a chiral or biaxial MM. Nevertheless, group theory, when properly applied, can be used to predict electric and magnetic behavior of MM inclusions for any incident field, including the existence and isotropic nature of the electromagnetic constitutive relationship. Using this framework, the fundamental properties of a MM design can be elucidated based on the symmetry class to which the unit cell belongs. This provides a methodology for the design of the electromagnetic properties of a MM, as described in Section 2. In Section 3, we introduce a new unit cell element called the "Zia" which offers similar inductive and capacitive paths as the SRR but with additional degrees of freedom for tuning its behavior and engineering a MM of a specific symmetry group. In Section 4, we demonstrate the design of a bianisotropic MM using the Zia element based on the inverse problem methodology described in Section 2. A validation of the bianisotropic behavior is presented through numerical simulations of the design and the retrieval of its electromagnetic properties. To further reinforce the power of the inverse group theory

methodology, the design of a chiral MM based on the Zia element and a validation of its behavior by numerical simulations is presented in Section 5, followed by a similar analysis of a biaxial MM Zia design in Section 6. Concluding remarks and discussions are given in Section 7.

2. GROUP THEORY APPROACH

Group theory has been used extensively in chemistry, where molecules are classified by symmetry and the spectroscopic or molecular orbital properties identified according to their symmetry groups [9]. This branch of chemistry has a number of similarities to electromagnetism that allow for well-developed concepts from that field to be applied analogously to MM design. In molecular spectroscopy, molecules are grouped according to their symmetry, with groups of the same symmetry exhibiting the same molecular vibrational modes. Thus, a molecule can be identified as, for example IR or Raman active, based solely on its symmetry group and without having to evaluate the actual modal solutions of the governing equations of motion.

By making the comparisons that molecules in chemistry are analogous to MM elements in electromagnetics and similarly that molecular normal modes of vibration are analogous to the fundamental resonant electrical current modes, we can apply the principles of symmetry and point groups to MM designs (Figure 1). Given these assumptions, the symmetry of a MM element is used to determine its point group, a character table is constructed based on the point group, and the generalized motion in terms of the normal modes of the element is found from the character table. A point group is a collection of all of the possibly symmetry elements of a MM element, and the corresponding character table is a matrix representation of the various symmetries represented by the point group. The details of the process for determining the point group of a molecule (MM element) is beyond the scope of this paper, but can be found in many chemistry textbooks [10]. As an example, a molecule belonging to the C_{2v} point group, which is the same symmetry group as a basic single SRR, is shown in Figure 2 along with the

corresponding character table. The first column on the table lists the point group symmetry under analysis (C_{2v}) and its irreducible representations. The following four columns list the symmetry operations of the C_{2v} point group and the corresponding characters, followed by the equivalent irreducible representations in linear and quadratic terms of the Cartesian coordinates in the last two columns. Figure 1 also illustrates the symmetry operations for the case of a simple C_{2v} molecule, for example H_2O. The character of the molecule expresses the symmetry adapted linear combinations, in terms of the irreducible representations. In molecular chemistry, this irreducible representation is combined with the matching atomic orbitals to generate the reducible representation corresponding to the symmetry-adapted linear combinations (SALCs) of orbitals for that molecule. When applied to MMs, the reducible representation corresponds to the active current modes of the MM element.

Given that group theory is based upon symmetry rules and symmetry operations, it imposes some restrictions on the system under analysis. First, in the case of MMs it assumes that incident electromagnetic fields are quasi-static. For the electromagnetic fields to be considered quasi-static, the unit cell dimension, a, has to be much smaller than the wavelength, λ, of the incident field, typically constrained as $a/\lambda < 10$. The commonly accepted explanation of the fundamental physics governing MMs is that their anomalous electromagnetic properties arise from resonances among the MM elements that give rise to effective constitutive parameters at the excitation wavelength [11]-[13]. Second, because the form of the governing Maxwell's equations, the solution of any electromagnetic problem strongly depends on its boundary conditions; if they are symmetric, the solution will also be symmetric. This transforms the problem into a boundary value problem where one can predict the symmetry properties of the solution without actually solving Maxwell's equations. As an example of this principle, group theory could be used to predict which field distributions are allowed between two infinite parallel conducting plates. Since any valid solution of the field has to have both vertical and horizontal

symmetries, as the parallel plates do, group theory can predict that field distributions having corresponding symmetries are allowed while asymmetric ones are not. Thus, group theory makes is possible to find the electric and magnetic properties of any shape without having to solve any equations of motion, as long as it posses symmetry and is a good conductor. Based on this group theory approach, the forward problem for determining the properties of a MM can be described by the following methodology. The symmetry point group of the MM is first determined based on symmetry operations, which specifies the character table of the symmetry group. This character table determines what electromagnetic behaviors are possible in the MM. The reducible representation of the MM topology is then calculated to determine which modes of the character table will actually be active, corresponding to the resonant current modes that can be coupled to as constrained by the type of excitation that is assumed. The response of the MM design can be confirmed by numerical simulations.

The power of this technique is fully revealed in the inverse problem approach, where the topology of the elements of a MM can be engineered from its desired electromagnetic constitutive tensor. The method, summarized in Figure 3, starts with the selection of a desired electromagnetic constitutive tensor, in which the tensor elements that are active (i.e., possibly nonzero for ζ, ξ, and off-diagonal ε and μ terms or possibly non-unity for diagonal ε and μ terms) can be specified, although their actual values cannot be determined by group theory alone but rather must be tuned by the geometrical and material properties of the actual MM elements. The chosen electromagnetic tensor mandates the form of the electromagnetic interactions that produce that behavior, which determines the linear and axial terms that must be present in the character table of the corresponding MM elements. This necessary set of terms allows for the elimination of symmetry groups that do not meet the desired electromagnetic response constraints, reducing the number of possible symmetry groups (the number of options remaining after the reduction may be only one). The symmetry group that is chosen (most often the one

having the least complexity) specifies the character table and hence symmetry operations that correspond to any MM element belonging to that symmetry group. Next, a MM element topology is chosen that belongs to the selected symmetry group, which can often be constructed of two or more simpler topologies of a closely related symmetry group (as an example, the case with the C_{2v} Zia geometry that is essentially composed of two C_2 Zia rings, described in detail in Section 3). The reducible representation of the MM element is calculated to ensure the activity of the requisite normal modes, which may mandate modification of the topology until the desired behavior is produced. The actual design topology can still take any form that has the correct geometrical symmetry, but is often further constrained by fabrication and/or simulation capabilities. Once a topology is selected, the electromagnetic constitutive tensor elements can be optimized through a cycle of simulating electromagnetic response of the resulting metamaterial and retrieving the tensor elements from the calculated *S* parameters.

The constitutive relationship between the electric and magnetic fields in many materials can be expressed as tensor of the following form:

$$\begin{bmatrix} \overline{D} \\ \overline{B} \end{bmatrix} = \begin{bmatrix} \overline{\overline{\varepsilon}} & \overline{\overline{\xi}} \\ \overline{\overline{\zeta}} & \overline{\overline{\mu}} \end{bmatrix} \begin{bmatrix} \overline{E} \\ \overline{H} \end{bmatrix}, \text{ where}$$
$$\overline{\overline{\varepsilon}} = \begin{bmatrix} \varepsilon_{xx} & \varepsilon_{xy} & \varepsilon_{xz} \\ \varepsilon_{yx} & \varepsilon_{yy} & \varepsilon_{yz} \\ \varepsilon_{zx} & \varepsilon_{zy} & \varepsilon_{zz} \end{bmatrix}, \tag{1}$$

with similar forms for the μ, ζ, and ξ sub-tensors. Here ε and μ are the regular tensor relations between the electric or magnetic flux density (***D*** and ***B***, respectively) and the electric or magnetic field intensity (***E*** and ***H***, respectively) typically referred to as the permittivity and permeability, respectively; while ζ and ξ are the crossed relations between flux densities and field intensities representing the magneto-electric effect. As an example of how these tensor elements can be determined, consider again the analogy between molecular orbitals and currents in MM elements. Since electric field is linear with current, it will transform under symmetry operations

as the position vector r, i.e. the linear Cartesian coordinates x, y, z. On the other hand, the magnetic field is axial with the current, and consequently will transform under the rotation R_x, R_y, R_z symmetry operations. Thus, the four quadrants of the electromagnetic constitutive tensor are accessed as shown in Figure 4, with the understanding that linear terms correspond to currents in straight wires that can interact with an incident electric field of suitable orientation, and axial terms correspond to current loops that can interact with an incident magnetic field of suitable orientation. The diagonal ε terms are provided by independent r modes (where r represents either x, y, or z), and diagonal μ terms by independent R_i modes (indicating the x, y, or z rotational modes); multiple terms that are not enclosed in parentheses indicate simultaneous, uncoupled modes. The ζ and ξ terms are provided by r_i,R_i modes (simultaneous linear and axial motions), and the off-diagonal ε and μ terms by (r_i,r_j) ($i \neq j$, i.e. coupled linear motions) and (R_i,R_j) ($i \neq j$, i.e. coupled rotational motions) modes, respectively. This interpretation differs from that of Ref. [7], which considered the r_i,r_j modes to be coupled linear motions, and did not provide interpretations for the (r_i,r_j) notation. To our understanding, this is an error on the behalf of the authors, where the (r_i,r_j) notation should indicate coupled linear motions (and hence off-diagonal ε and μ terms) and the r_i,r_j notation should indicate multiple independent linear motions that exist for a single mode of a symmetry group. This can be understood intuitively by considering that it is not physically meaningful for linear and rotational modes to be coupled, hence r_i,R_i modes are never seen enclosed in parentheses.

3. ZIA METAMATERIAL

To alleviate the limitations of the SRR design, we have developed a design that retains much of the ease of fabrication inherent in the SRR, while adding the ability to independently modify the electric and magnetic response. In addition, the topology of our design maintains the

inductive and capacitive paths of the SRR, which give rise to electrical and magnetic resonances, respectively, while providing additional degrees of freedom for tailoring the symmetry properties of the element, and hence the MM constructed from it. This design, based on a well-known geometry called the Zia [14] shown in Figure 5, was chosen because it combines a ring structure that gives it inductance with tunable capacitances across the arms that intersect the ring. While the SRR design has the benefits of relatively easy fabrication and simulation, it is limited by its topology to only a few degrees of freedom, primarily the gap width and the metal trace thickness. This limitation makes is difficult to tune the electric response of the MM without simultaneously changing the magnetic behavior, thus limiting the functionality of the device.

The Zia design can have essentially infinite variants, such as the C_{2h} and C_{2n} examples shown in Figure 5. Additionally, two or more Zia rings of one symmetry can be combined to create a design belonging to a symmetry group; the design marked as C_{2v} in Figure 5 consists of two C_{2h} symmetry rings, stacked on top of each other in the planar direction, with one ring rotated by an angle of 90º with respect to the other. This design allows for tuning of the electrical resonance, by altering the capacitive arms intersecting the ring in length and/or number, independently of the magnetic resonance, which can be tuned by changing the radius of the ring and/or adding more than one concentric ring. Thus, the electric and magnetic resonances of the inclusions, and consequently the resonance of the MM, can be aligned without rotating the polarization.

To illustrate the power of this group theory design methodology [15], we detail the design of three different metamaterial elements with engineered electromagnetic behavior and all based on this Zia element, with focus on the application of the inverse problem solution to each MM design. The highlighted examples include bianisotropic, chiral, and biaxial metamaterials.

4. DESIGN AND SIMULATION OF A BIANISOTROPIC METAMATERIAL

Of particular interest in the realm of MMs is the possibility of constructing a bianisotropic material [16], in which the electric and magnetic fields are coupled and the coupling depends on the direction of the incident wave, since such a material is a promising candidate for creating a left-handed MM. Assuming that reciprocity holds, i.e. $\zeta^T = -\xi$, a possible electromagnetic constitutive relationship that describes a bianisotropic material can be written as [17]:

$$\begin{bmatrix} \overline{\overline{\varepsilon}} & \overline{\overline{\xi}} \\ \overline{\overline{\zeta}} & \overline{\overline{\mu}} \end{bmatrix} = \begin{bmatrix} 1 & 0 & 0 & 0 & \xi_{xy} & 0 \\ 0 & 1 & 0 & \xi_{yx} & 0 & 0 \\ 0 & 0 & \varepsilon_{zz} & 0 & 0 & 0 \\ 0 & -\xi_{yx} & 0 & 1 & 0 & 0 \\ -\xi_{xy} & 0 & 0 & 0 & 1 & 0 \\ 0 & 0 & 0 & 0 & 0 & \mu_{zz} \end{bmatrix}. \tag{2}$$

Based on the argument made in the previous section, Eq. (2) implies that the corresponding symmetry group must have r , R, and r_i,R_j modes, specifically z; R_z; x,R_y; and y,R_x, where an electric field in the y-direction yields a magnetic field in the x-direction and vice versa. The C_{2v} group is simplest symmetry group that fits the necessary specifications for these required linear/axial modes, as can be seen from the character table in Figure 2. As mentioned in the previous section, the Zia design shown in Figure 5 can be engineered such that it falls into the C_{2v} symmetry category, and hence should demonstrate the bianisotropic behavior we seek. To illustrate how suitable MM element belonging to this group can be designed, we start with the Zia element and follow the decision chart shown in Figure 6. The unaltered Zia element by itself is immediately excluded from the first two sets of groups, those of low and high symmetry. A single Zia ring has a C_2 axis as its highest-order rotation axis, but is also has a perpendicular C_2 axis that designates it as a D group symmetry. To break this rotational axis, a second identical Zia ring is stacked centered with the first ring but rotated by 90°. Since this design (far right of

Figure 5) clearly does not have a horizontal mirror symmetry plane, it satisfies the requirements for the C_{2v} symmetry group.

To find the resonant modes of the Zia design, each symmetry operation of the character table of the C_{2v} point group must be applied to a set of basis currents chosen for a given Zia design. The basis vectors can be represented as current segments of the simplified Zia topology, as shown in Figure 7 for a given set of assumed bases. Next, the effect of each symmetry operation on the current basis elements can be tabulated, as shown in Table 1, and the number of

Table 1. Effect of C_{2v} Symmetry Operations on the Current Basis Elements

C_{2v}	e_1	e_2	e_3	e_4	e_5	e_6	e_7	e_8	e_9	e_{10}	e_{11}	e_{12}	e_{13}	e_{14}	e_{15}	e_{16}	e_{17}	e_{18}	e_{19}	e_{20}	χ_Γ
E	e_1	e_2	e_3	e_4	e_5	e_6	e_7	e_8	e_9	e_{10}	e_{11}	e_{12}	e_{13}	e_{14}	e_{15}	e_{16}	e_{17}	e_{18}	e_{19}	e_{20}	20
C_2	e_6	e_7	e_8	e_9	e_{10}	e_1	e_2	e_3	e_4	e_5	e_{16}	e_{17}	e_{18}	e_{19}	e_{20}	e_{11}	e_{12}	e_{13}	e_{14}	e_{15}	0
σ_{xz}	$-e_5$	$-e_4$	$-e_3$	$-e_2$	$-e_1$	$-e_{10}$	$-e_9$	$-e_8$	$-e_7$	$-e_6$	$-e_{20}$	$-e_{19}$	$-e_{18}$	$-e_{17}$	$-e_{16}$	$-e_{15}$	$-e_{14}$	$-e_{13}$	$-e_{12}$	$-e_{11}$	-2
σ_{yz}	$-e_{10}$	$-e_9$	$-e_8$	$-e_7$	$-e_6$	$-e_5$	$-e_4$	$-e_3$	$-e_2$	$-e_1$	$-e_{15}$	$-e_{14}$	$-e_{13}$	$-e_{12}$	$-e_{11}$	$-e_{20}$	$-e_{19}$	$-e_{18}$	$-e_{17}$	$-e_{16}$	-2

times each irreducible representation occurs, a_m, calculated as:

$$a_m = \frac{1}{h}\sum_i n_i \chi(i)\chi_m(i) \tag{3}$$

where h is the number of symmetry operations in the point group, n_i is number of symmetry operations in each class i, χ is the character of a reducible representation, and χ_m is character of the irreducible representation. This calculation performed for the Zia design represented in Figure 7 results in a reducible representation that can be written as $\Gamma = 4A_1 + 6A_2 + 5B_1 + 5B_2$. The modes of the Zia design are generated by applying the symmetry operations, as shown in the following expression

$$\begin{bmatrix} \varphi'(A_1) \\ \varphi'(A_2) \\ \varphi'(B_1) \\ \varphi'(B_2) \end{bmatrix} = \begin{bmatrix} 1 & 1 & 1 & 1 \\ 1 & 1 & -1 & -1 \\ 1 & -1 & 1 & -1 \\ 1 & -1 & -1 & 1 \end{bmatrix} \bullet \tag{4}$$

$$\begin{bmatrix} e_1 & e_2 & e_3 & e_4 & e_5 & e_6 & e_7 & e_8 & e_9 & e_{10} & e_{11} & e_{12} & e_{13} & e_{14} & e_{15} & e_{16} & e_{17} & e_{18} & e_{19} & e_{20} \\ e_6 & e_7 & e_8 & e_9 & e_{10} & e_1 & e_2 & e_3 & e_4 & e_5 & e_{16} & e_{17} & e_{18} & e_{19} & e_{20} & e_{11} & e_{12} & e_{13} & e_{14} & e_{15} \\ -e_5 & -e_4 & -e_3 & -e_2 & -e_1 & -e_{10} & -e_9 & -e_8 & -e_7 & -e_6 & -e_{20} & -e_{19} & -e_{18} & -e_{17} & -e_{16} & -e_{15} & -e_{14} & -e_{13} & -e_{12} & -e_{11} \\ -e_{10} & -e_9 & -e_8 & -e_7 & -e_6 & -e_5 & -e_4 & -e_3 & -e_2 & -e_1 & -e_{15} & -e_{14} & -e_{13} & -e_{12} & -e_{11} & -e_{20} & -e_{19} & -e_{18} & -e_{17} & -e_{16} \end{bmatrix}$$

where φ' represents a mode of the element. Finally, the four modes represented in the reducible representation are shown in Figure 8 for one of the equivalent topologies possible as allowed by the C_{2v} point group symmetry operations. Note that group theory guarantees that if either the electric or magnetic field is coupled and resonates, the other field (either magnetic or electric) will be coupled and resonate as well, ensuring that both effects will be tied together and thus occur at the same frequency.

To test the validity of the behavior predicted by group theory, simulations of the Zia design were performed using the commercial software package CST Microwave Studio™. The frequency domain solver was used for this application, with unit cell (i.e. periodic) boundary conditions implemented to simulate an infinitely large sheet in the in-plane directions of the MM. The single-layer thick Zia structure was modeled with 1μm thick traces composed of gold in air as host material; with nominal dimensions listed in Table 2 corresponding to the parameters in Figure 9. Plane waves were launched perpendicular to the MM the sheet from both sides and using in two polarizations: vertical linear and horizontal linear. Although at the wavelength of excitation the MM appears essentially identical from either side of the sheet, both

Table 2. Dimensions of Zia element parameters shown in Figure 9.

Parameter	**d**	**r_{ir}**	**f_w**	**f_l**	**f_g**	**r_w**	**period, *a***	**side**
Dimension	50μm	100μm	10μm	100μm	1μm	10μm	$4r_{ir}$ = 400μm	0 (centered)

ports were allowed to be the source to verify the reciprocity of the MM. Same-polarization and cross-polarization terms were also calculated to study whether the design preserves the incident polarization or imposes an abnormal polarization rotation. Thus, a total of sixteen S-parameters

results were calculated for each two-port simulation, four corresponding to the various S-parameters for each polarization multiplied by the four possible self- and cross-polarization permutations. Each parameter has the form $S_{i,p,j,q}$, where i represents the output port number (1 or 2), p represents the polarization measured at the output port (vertical or horizontal), j represents the input port number (1 or 2), and q represents the polarization radiated at the input port (vertical or horizontal); for instance, $S_{2,v,1,h}$ represents the transmission coefficient from port 1 radiating a horizontally polarized wave to port 2 detecting a vertically polarized wave. Since according to Eq. (2) the polarization of an incoming wave is preserved by this MM (no rotation of polarization), it is expected that $S_{i,p,j,q} \approx 0 \quad \forall i,j,p \neq q$. Furthermore, since this is a passive MM possessing C_{2v} symmetry, we can further predict that $S_{i,p,j,p} \approx S_{j,q,i,q} \quad \forall p,q,i \neq j$ and $S_{i,p,i,p} \approx S_{j,q,j,q} \quad \forall p \neq q, i \neq j$. This behavior can be deduced from Figure 10, where the simulated S-parameters are plotted for frequencies from 67-800GHz. Three groups of terms can clearly be distinguished: the two same-polarization groups, between 0dB and roughly -30dB; and the cross-polarization group, below -30dB.

As mentioned in the previous section, group theory predicts bianisotropic behavior for a MM with elements having C_{2v} symmetry; however, no actual information is provided about either the existence of resonances or their location in the EM spectrum. In fact, the case could exist where no resonances are found in the effective medium regime (i.e. where the unit cell period $<< \lambda_{\text{incident}}$), resulting in a design with no actual MM behavior. To better understand why no resonances appeared for this design in the effective medium regime, the Zia element currents from the simulations, shown in Figure 11, were compared with the mode predictions in Figure 8. The calculated currents agree with the predictions as expected, and highlight the reason for the lack of resonance in the structure. As seen in Figure 11, there is no current circulation around the Zia due to lack of return path for the current to form a closed loop. Instead, currents travel

upwards on both sides of the structure to accumulate positive charges on the top during one half period, then travel downwards to accumulate positive charges at the bottom during the other half period. Thus, to achieve a net current flow while preserving the C_{2v} symmetry, a bisecting rod was added to the design as illustrated in Figure 12, giving rise to two current loops. Currents are allowed to circulate by means of the capacitances provided by the fingers of the modified Zia design and can now be excited by an incident electric field via the central "antenna" rod, while the loop itself supplies a path for inductance and coupling to a magnetic field. Using this design that provides both a capacitive on the upper Zia ring and an inductive path on the lower ring, resonant is guaranteed with its location in frequency dependent only on the physical dimensions of the modified Zia, namely, the thicknesses and lengths of the fingers and rings, and the separations among the fingers and rings. It has been previously reported that an electric field that crosses the gaps (perpendicular to the gaps) is necessary to obtain a resonance [18]. However, this turns out to be highly dependent of the topology of the MM element; resonant behavior is more dependent on symmetry of the paths parallel to the electric field than the orientation of the capacitive gaps. In fact, the existence and intensity of a resonance depends upon the shape of the paths that form the loop which the current flows around. If a closed path that is asymmetric with respect to the electric field can be found, a current will flow around it; and if a gap (or capacitance) exists along the path, a resonance, and hence MM behavior, is possible. Thus, a resonance can be observed despite the fact that the electric field is oriented parallel to the capacitive gaps instead of crossing them. This effect explains the appearance of currents on the right ring in Figure 12 and not on the left ring.

The values of the four constitutive relations of the MM were obtained using a retrieval code that was developed to extract these values from the calculated S-parameters. Since it is assumed that the Zia MM design is generally bianisotropic, a simple isotropic retrieval code is not suitable. Thus, a code was developed that is able to recover the refractive index n and the

input impedance Z for both directions of propagation, as long as they are perpendicular to the faces of the MM. This is significant because although the Zia MM is reciprocal and thus has identical forward and backward refractive indices, the forward and backward wave impedances need not be the same. The impedance and can be calculated directly as:

$$\mp Z_{\pm} = \frac{-(r_{+} - r_{-}) \pm \sqrt{(r_{+} - r_{-})^2 + [(1 - r_{+})(1 - r_{-}) - t_{-}t_{+}][(1 + r_{-})(1 + r_{+}) - t_{-}t_{+}]}}{(1 - r_{+})(1 - r_{-}) - t_{-}t_{+}}, \tag{5}$$

where t refers to transmission coefficients and r refers to reflection coefficients, and the refractive index can be found through the relationship:

$$\cos(kn_{\pm}d) = \frac{1}{2}\left[\frac{(1 \pm Z_{\pm})t_{-}}{1 + r_{-} \pm Z_{\pm}(1 - r_{-})} + \frac{(1 \mp Z_{\pm})t_{+}}{1 + r_{+} \mp Z_{\pm}(1 - r_{+})}\right], \tag{6}$$

where k is the wave number and d is the thickness of the MM layer; care should be taken to ensure that the correct branch is chosen when inverting the cosine function. Note that the transmission and reflection coefficients are directly related to the S-parameters as $t_{-} = S_{12}$, $t_{+} = S_{21}$, $r_{+} = S_{11}$, and $r_{-} = S_{22}$. The constitutive parameters ε_{xx}, μ_{zz}, ξ_{xy}, and ζ_{yx} can be found for a wave with perpendicular incidence from the impedance and refractive index as:

$$\varepsilon_r = \frac{n_{+} + n_{-}}{Z_{+} + Z_{-}} \tag{7}$$

$$\mu_r = \frac{n_{+} + n_{-}}{Z_{+} + Z_{-}} Z_{+} Z_{-} \tag{8}$$

$$\xi_{xy} = \frac{\sqrt{\mu_0 \varepsilon_0}}{2}\left[(n_{+} - n_{-}) - \left(\frac{Z_{+} - Z_{-}}{Z_{+} + Z_{-}}\right)(n_{+} + n_{-})\right] \tag{8}$$

$$\zeta_{xy} = \frac{\sqrt{\mu_0 \varepsilon_0}}{2}\left[(n_{+} - n_{-}) + \left(\frac{Z_{+} - Z_{-}}{Z_{+} + Z_{-}}\right)(n_{+} + n_{-})\right], \tag{8}$$

where μ_0 is the free-space permeability and ε_0 is the free-space permittivity.

A series of CST simulations were run to study the topological scaling behavior of the modified Zia design and verify that resonances occur as expected due to the asymmetry of the

current paths parallel to the electric field. The values of the constitutive parameters were calculated using the retrieval code for each topology. First, an excitation at perpendicular incidence was used to probe the bianisotropic character of the modified Zia MM, as shown in Figure 13(a), with the values of f_l, r_{ir}, and d (see Figure 9) scaled independently from their initial values of 100μm, 125μm, and 50μm, respectively. Resonant behavior is clearly evident in the refractive index (Figure 13(b), (d), and (f)) and impedance (Figure 13(c), (e), and (g)) response of the MM. The refractive index increases as expected as f_l is increased from 50μm to 139μm (Figure 13(b)), since increasing the finger length effectively increases the capacitance of the Zia ring. Correspondingly, the impedance, being inversely proportional to the capacitance, decreases as f_l is increased (Figure 13(c)). The wavelength is proportional to the capacitance as well as the inductance, and thus increases with increasing f_l (Figure 13(b) and (c)), and as r_{ir} is increased from 75μm to 125μm (Figure 13(d) and (e)), since increasing Zia ring radius effectively increases the inductance of the MM. In addition, the retrieved values in each figure are plotted for normal incidence from both the top (solid curves) and the bottom (dashed curves), demonstrating the reciprocal nature of this MM. It is noted, no resonance appears for d = 10μm, and saturation of the tuning seen for d > 50μm (Figure 13(f) and (g)). However, much more interesting is that the resonant frequency shifts in the opposite direction as d is increased as f_l or r_{ir} indicating that the separation between the Zia rings can be used as a tuning parameter with opposite behavior from the other design parameters yielding an added degree of freedom for tuning.

Next, the same parameter sweeps were performed with the excitation parallel to the plane of the modified Zia rings, as shown in Figure 14(a). Resonant behavior is again observed, with much larger shifts in the resonant frequency as the topological parameters are changed, particularly for d (Figure 14(f) and (g)), where resonant behavior is seen for all values. The refractive index and impedance values exhibit similar tuning, although with significantly larger

magnitudes, most notable the imaginary parts. Also, the inductive coupling is now much stronger due to the alignment of the magnetic field perpendicular to the plane of the Zia rings, resulting in larger refractive index and impedance values and an increasing trend as r_{ir} is increased (Figure 13(e)). The shift in resonant wavelength with d again appears to saturate above d = 50μm (Figure 14(f) and (g)), but has a stronger effect due the orientation. This again offers an additional degree of freedom in tuning the behavior of the MM, and effectively relaxes the constraints for fabrication, since the resonant frequency can be shifted over a relatively large range without having to change the period of the MM.

Since group theory predicts bianisotropic behavior only for perpendicular incidence, it is also possible to verify the model by checking for the absence of bianisotropic response for parallel incidence. Thus, ξ_{xy}, and ζ_{yx} were calculated for various values of r_{ir} for both perpendicular (Figure 15(a) and (b), respectively) and parallel (Figure 15(c) and (d), respectively) excitation. Although at first glance there appears to be resonant behavior for parallel incidence, the parameter values are nearly two orders of magnitude smaller than the corresponding values for perpendicular incidence, thus confirming the lack of bianisotropy. Also note that the wavelength again increases with r_{ir}, as well as ξ_{xy}, and ζ_{yx}, being the directly proportional to the impedance.

The addition of the bisecting rod resulted in a clear resonance within the effective medium regime of the MM, which confirms the necessity of a return path for the currents to form a closed loop. The MM behavior is clearly demonstrated by the artificial values of permittivity and permeability obtained, as evidenced by the artificial indices of refraction that vary over a range as large as $0.1<n<5$ for both perpendicular and parallel incidence.

5. DESIGN AND SIMULATION OF A CHIRAL METAMATERIAL

In addition to bianisotropic behavior, metamaterials exhibiting chiral behavior have elicited much interest. To demonstrate the power of the inverse group theory approach, in this section we outline the process for design of a chiral MM element. In such materials, the direction of polarization of linearly polarized light is rotated as the beam propagates through the material, or alternatively, left circular polarized light with have a different transmission coefficient through the material than right circular polarized light. An example of an electromagnetic constitutive relationship for a chiral material is given in Eq. (9), from which it can be deduced that the corresponding symmetry group must have r_i,R_i modes, i.e. r_x,R_x; r_y,R_y; and r_z,R_z.

$$\begin{bmatrix} \overline{\overline{\varepsilon}} & \overline{\overline{\xi}} \\ \overline{\overline{\zeta}} & \overline{\overline{\mu}} \end{bmatrix} = \begin{bmatrix} \varepsilon_{xx} & 0 & 0 & \xi_{xx} & 0 & 0 \\ 0 & \varepsilon_{yy} & 0 & 0 & \xi_{yy} & 0 \\ 0 & 0 & \varepsilon_{zz} & 0 & 0 & \xi_{zz} \\ \xi_{xx} & 0 & 0 & \mu_{xx} & 0 & 0 \\ 0 & \xi_{yy} & 0 & 0 & \mu_{yy} & 0 \\ 0 & 0 & \xi_{zz} & 0 & 0 & \mu_{zz} \end{bmatrix}. \tag{9}$$

The simplest symmetry group that fits the necessary specifications is D_2; the character table of this group is shown in Figure 16(a).

To design a suitable MM element belonging to this group, we will start with the Zia element and follow the decision chart shown in Figure 6. The Zia element by itself is immediately excluded from the first two sets of groups, those of low and high symmetry. Since a cube element topology is desired to enable stacking for a complete 3D MM, the C_3 axes inherent in the cube geometry must be broken; this was done by rotating the Zia rings on the faces perpendicular to the *x*- and *y*-directions by 45° in alternating directions, as shown in Figure 16(b). The highest-order rotation axis is now a C_2 axis, and since we want *D* group symmetry at least one other perpendicular C_2 axis must be preserved. Next, any horizontal mirror planes must be eliminated to avoid the D_{nh} groups, while maintaining a perpendicular C_2 axis. This was

achieved by adding 90° bends to the extended fingers of the Zia design in opposite directions top and bottom, as shown in Figure 16(b), and then placing the Zia elements centered on the six faces of a cube but rotated 180° with respect to the central rod, thus restoring the perpendicular rotation axes without adding any mirror symmetry planes. This final design clearly does not have a diagonal mirror symmetry plane, thus satisfying the requirements for the D_2 symmetry group. As shown in the character table in Figure 16(a), chiral behavior requires the activity of all of the B modes (i.e. B_1, B_2, and B_3). Following the approach outlined in the previous section, a calculation of the reducible representation of this Zia MM element, $\Gamma = 3A_1+5B_1+5B_2+5B_3$, indicates that all 4 modes are active and thus chiral behavior is possible.

Next, the chiral MM design was simulated using CST Microwave Studio™ to confirm the presence of the specified behavior. The field plot of electrical current on the MM elements, shown in Figure 17, verifies that the Zia elements are in fact excited by left or right circular polarized incident radiation. The Zia elements in this case already include the central rod added to the bianisotropic design, to ensure that the electric field could couple to the metal traces and generate currents. The plots in Figure 18(a) show the transmission and reflection for the two polarizations with incidence from the front and the back of the MM cube. As expected, the transmission (reflection) in the same direction differs for the left circular polarized beam as compared with the right circular polarized beam, indicating chiral behavior. Also, the transmission (reflection) with opposite incident directions for the two polarizations is the same, indicating that this MM is not symmetric with respect to the left- and right-hand orientations. Similar behavior is seen for in the plots of the phase for the transmitted and reflected beams, shown in Figure 18(b), confirming that it is indeed a chiral material.

6. DESIGN AND SIMULATIONS OF A BIAXIAL METAMATERIAL

As a final example, another metamaterial having electromagnetic tensor corresponding to a biaxial, or trirefringent, material is designed here. In such a material, the index of refraction experienced by an incoming beam of light depends on the angle of incidence and state of polarization of the beam, with three independent values possible. An example electromagnetic constitutive tensor for a biaxial material is given in Eq. (10), which corresponds to a symmetry group having at least 2 r_i modes and two R_i modes, in this case r_x; r_y; R_x; and R_y; all of which must be independent. The symmetry point group corresponding to this behavior that will be used here is D_{2h}, as shown in Figure 19(a).

$$\begin{bmatrix} \overline{\overline{\varepsilon}} & \overline{\overline{\xi}} \\ \overline{\overline{\zeta}} & \overline{\overline{\mu}} \end{bmatrix} = \begin{bmatrix} \varepsilon_{xx} & 0 & 0 & 0 & 0 & 0 \\ 0 & \varepsilon_{yy} & 0 & 0 & 0 & 0 \\ 0 & 0 & 1 & 0 & 0 & 0 \\ 0 & 0 & 0 & \mu_{xx} & 0 & 0 \\ 0 & 0 & 0 & 0 & \mu_{yy} & 0 \\ 0 & 0 & 0 & 0 & 0 & 1 \end{bmatrix}. \tag{10}$$

The design of this MM element again begins with the Zia element. Following the decision chart shown in Figure 6, an element is desired that belongs to neither a low nor high symmetry group and has one or more rotational axes perpendicular to its C_2 axis, thus making it a D group. As with the previous designs, a cube element topology is desired here, which again required breaking of the C_3 axis symmetries by rotating the Zia rings on the faces perpendicular to the x- and y-directions by 45° in alternating directions, as shown in Figure 19(b). However, diverging from the chiral design described above, we now want a horizontal mirror plane to satisfy the D_{2h} group symmetry requirements, which is already accomplished by basic Zia design for the two parallel rings. The final modification is to place the Zia elements on the six faces of a cube to create a stackable 3D structure, since otherwise the MM will be constrained to a planar-only topology. Aligning each opposing Zia pair with the rods aligned, as shown in Figure 19(b), ensures that all rotational axes and mirror planes are preserved. Once again, by analogy to the

calculation performed previously, the resulting reducible representation of this MM element is $\Gamma=3A_g+5(B_{1g}+B_{2g}+B_{3g})+4(B_{1u}+B_{2u}+B_{3u})$, which clearly contains all of the B modes that necessary to enable biaxial behavior.

The biaxial MM design was also simulated using CST to verify the specified behavior. The field plot of electrical current on the MM elements, shown in Figure 20, verifies that the Zia elements are in fact excited linearly polarized incident radiation. In such a material, an incident beam that is linearly polarized with the polarization aligned with the principle axes of the material will maintain its state of polarization but experience a different refractive index depending on the principle axis of the material to which it is aligned. However, if the polarization is aligned at an angle between the principle axes, the incident linear polarized light will leave the material with an altered polarization state after propagation through it, exiting with generally elliptical polarization. This change of polarization can be observed in Figure 21, where the field vectors of the beam exiting the MM under linearly polarized incident radiation can be seen to be rotating during each cycle of the electromagnetic oscillation, indicating elliptical polarization and hence biaxial behavior of the material.

Finally, to avoid the issues of ill-defined problems and cost functions, we have listed the various groups with the possible corresponding behaviors in Table 1 to demonstrate that while other functionalities may be possible, only the behaviors identified with a specific group are well-defined from a group theoretical inverse design point of view. In addition, the demonstration of a given behavior is subject to the activity of the necessary modes of the symmetry group. Thus, there are 48 groups with corresponding possible functionalities; if a desired behavior falls outside these functionalities, the design may represent a nonphysical problem and at a minimum be ill defined in terms of a group theory design approach.

7. CONCLUSIONS

It has been demonstrated that group theory can be an invaluable framework for designing MM structures, enabling the prediction of electromagnetic behavior and modal activity based on the MM element unit cell alone. However, we have shown that the real strength of group theory applied to MM design lies in the ability to address the inverse design problem, narrowing the infinite choice of possible MM element to a defined set of symmetry choices based on the choice of a desired electromagnetic constitutive relationship. We also introduced the Zia element as a flexible and practical topology from which to build an arbitrary MM design. The power of the inverse problem solution via group theory was demonstrated with the design of a bianisotropic, chiral, and biaxia MM, using the Zia design template as the starting point. The value of the Zia MM was highlighted for the bianisotropic design, where it provided several degrees of freedom that allowed for engineering of tailored refractive index and impedance values over a relatively wide range of frequencies, with demonstrated tuning of the refractive index from 2.5 at $\lambda \approx$ 2200μm (135GHz) to 4 at $\lambda \approx$ 3500μm (85GHz).

Simulations confirmed that strong coupling between electric and magnetic fields was achieved for our bianisotropic MM at a resonance frequency and perpendicular incidence that was absent at parallel incidence, confirming the behavior of the design. Simulation results for the chiral MM showed the characteristic difference in transmission amplitude and phase for right-handed vs. left-handed polarization. Also, the rotation of polarization resulting in off-axis linear polarization converting to elliptical polarization inherent in biaxial materials was evidenced our biaxial MM design. Thus, this group theory approach to the inverse MM design problem represents a formidable technique for the design and optimization of MM devices.

8. ACKNOWLEDGEMENTS

The authors would like to acknowledge the help of Dr. Larry Warne and Dr. Lorena Basilio from Sandia National Laboratories for providing the bianisotripic retrieval code used in this paper, as well as the useful and valuable discussions. Sandia National Laboratories is a multi-program laboratory managed and operated by Sandia Corporation, a wholly owned subsidiary of Lockheed Martin Corporation, for the U.S. Department of Energy's National Nuclear Security Administration under contract DE-AC04-94AL85000.

REFERENCES

[1] R. A. Shelby, D. R. Smith, and S. Schultz, "Experimental verification of a negative index of refraction," S*cience* **292**, 77 (2001).

[2] V.G. Veselago, "The electrodynamics of substances with simultaneously negative values of ε and μ," *Sov. Phys. - Uspekhi* **10**, 509 (1968).

[3] J. B. Pendry, "Negative refraction makes a perfect lens," *Phys. Rev. Lett.* **85,** 3966 (2000).

[4] K. B. Alici and E. Özbay, "Radiation properties of a split ring resonator and monopole composite," *Phys. Status Solidi B* **244**, 1192 (2007).

[5] J. B. Pendry, D. Schurig, and D. R. Smith, "Controlling electromagnetic fields," *Science* **312**, 1780 (2006).

[6] J. B. Pendry, A. J. Holden, D. J. Robbins, and W. J. Stewart, "Magnetism from conductors and enhanced nonlinear phenomena," *IEEE Trans. Microwave Theory Tech.* **47**, 2075 (1999).

[7] W. J. Padilla, "Group theoretical description of artificial electromagnetic metamaterials", *Opt. Express* **15**, 1639 (2007).

[8] N. Wongkasem, A. Akyurtlu, and K. A. Marx, "Group theory based design of isotropic negative refractive index metamaterials," *Prog. Electromag. Res.* **63**, 295 (2006).

[9] F. A. Cotton, *Chemical Applications of Group Theory,* 3rd ed., (John Wiley & Sons, New York, 1990).

[10] G. L. Miessler and D. A. Tarr, *Inorganic Chemistry*, 4th ed., (Prentice Hall, New Jersey, 2011).

[11] D. R. Smith, D. C. Vier, Th. Koschny, and C. M. Soukoulis, "Electromagnetic parameter retrieval from inhomogeneous metamaterials," *Phys. Rev. E* **71**, 036617 (2005).

[12] X. Chen, B.-I. Wu, J. A. Kong, and T. M. Grzegorczyk, "Retrieval of the effective constitutive parameters of bianisotropic metamaterials," *Phys. Rev. E* **71**, 046610 (2005).

[13] C. Menzel, C. Rockstuhl, T. Paul, F. Lederer, and T. Pertsch, "Retrieving effective parameters for metamaterials at oblique incidence," *Phys. Rev. B* **77**, 195328 (2008).

[14] The word "Zia" comes from the name of a Native American tribe in New Mexico who regarded the Sun as a sacred; their Zia Sun Symbol is featured on the New Mexico state flag. Coincidentally, Zia is also a male Arabic name meaning "light" (as from a luminous object).

[15] I. El-Kady and C. M. Reinke, "Metamaterial with Tailorable Electromagnetic Properties," U.S.A., patent pending.

[16] G. P. Bava, "General form of the reciprocity relationship for bianisotropic media," *Electron. Lett.* **4**, 299 (1968).

[17] I. V. Lindell, A. H. Shivola, S. A. Tratyakov, and A. J. Viitanen, *Electromagnetic Waves in Chiral and Bi-Isotropic Media*, (Artech House, Inc., Massachusetts, 1994).

[18] N. Katsarakis, T. Koschny, M. Kafesaki, E. N. Economou, and C. M. Soukoulis, "Electric coupling to the magnetic resonance of split ring resonators," *Appl. Phys. Lett.* **84**, 2943 (2004).

LIST OF TABLES

LIST OF FIGURES

Figure 12. (Color) Modified Zia element design, demonstrating the closed current path and central rod, which allows for coupling to an incident electric field that is parallel to the rod.

Figure 13. (Color) a. Schematic of the modified Zia element with an excitation at normal incidence. Frequency response of b. the refractive index and c. impedance as fl is varied from 50μm to 139μm with rir = 125μm and d = 50μm. Frequency response of d. the refractive index and e. impedance as rir is varied from 75μm to 125μm with fl =100μm and d = 50μm. Frequency response of f. the refractive index and g. impedance as d is varied from 10μm to 100μm with fl =100μm and rir = 125μm.

Figure 14. (Color) a. Schematic of the modified Zia element with an excitation at parallel incidence. Frequency response of b. the refractive index and c. impedance as f_l is varied from 50μm to 139μm with r_{ir} = 125μm and d = 50μm. Frequency response of d. the refractive index and e. impedance as r_{ir} is varied from 75μm to 125μm with f_l =100μm and d = 50μm. Frequency response of f. the refractive index and g. impedance as d is varied from 10μm to 100μm with f_l =100μm and r_{ir} = 125μm.

Figure 15. (Color) Frequency response of a. ξ_{xy}, and b. ζ_{yx} for the modified Zia metamaterial with normal incidence as r_{ir} is varied from 75μm to 125μm with f_l =100μm and d = 50μm. Frequency response of c. ξ_{xy}, and d. ζ_{yx} for the modified Zia metamaterial with parallel incidence as r_{ir} is varied from 75μm to 125μm with f_l =100μm and d = 50μm.

Figure 16. (Color online) a. Character table of the D_2 group, the simplest symmetry group that fits the necessary specifications for a chiral MM. b. A corresponding element design based on the Zia ring.

Figure 17. (Color) Field plot of electrical current on the chiral MM elements, verifying that the Zia elements are in fact excited by left or right circular polarized incident radiation.

Figure 18. (Color) a. Transmission and reflection for left and right circular polarizations with incidence from the front and the back of the chiral MM cube. b. Phase of the transmitted and reflected waves corresponding to the plots in a.

Figure 19. (Color online) a. Character table of the D_{2h} group, a symmetry group that fits the necessary specifications for a biaxial MM. b. A corresponding element design based on the Zia ring.

Figure 20. (Color) Field plot of electrical current on the biaxial MM elements, verifying that the Zia elements are in fact excited linearly polarized incident radiation.

Figure 21. (Color) Field vectors of the beam exiting the MM under linearly polarized incident, where the field vectors can be seen to be rotating during each cycle of the electromagnetic oscillation at **a.** 45°, **b.** 135°, **c.** 225°, and **d.** 315°, indicating elliptical polarization and hence biaxial behavior of the material.

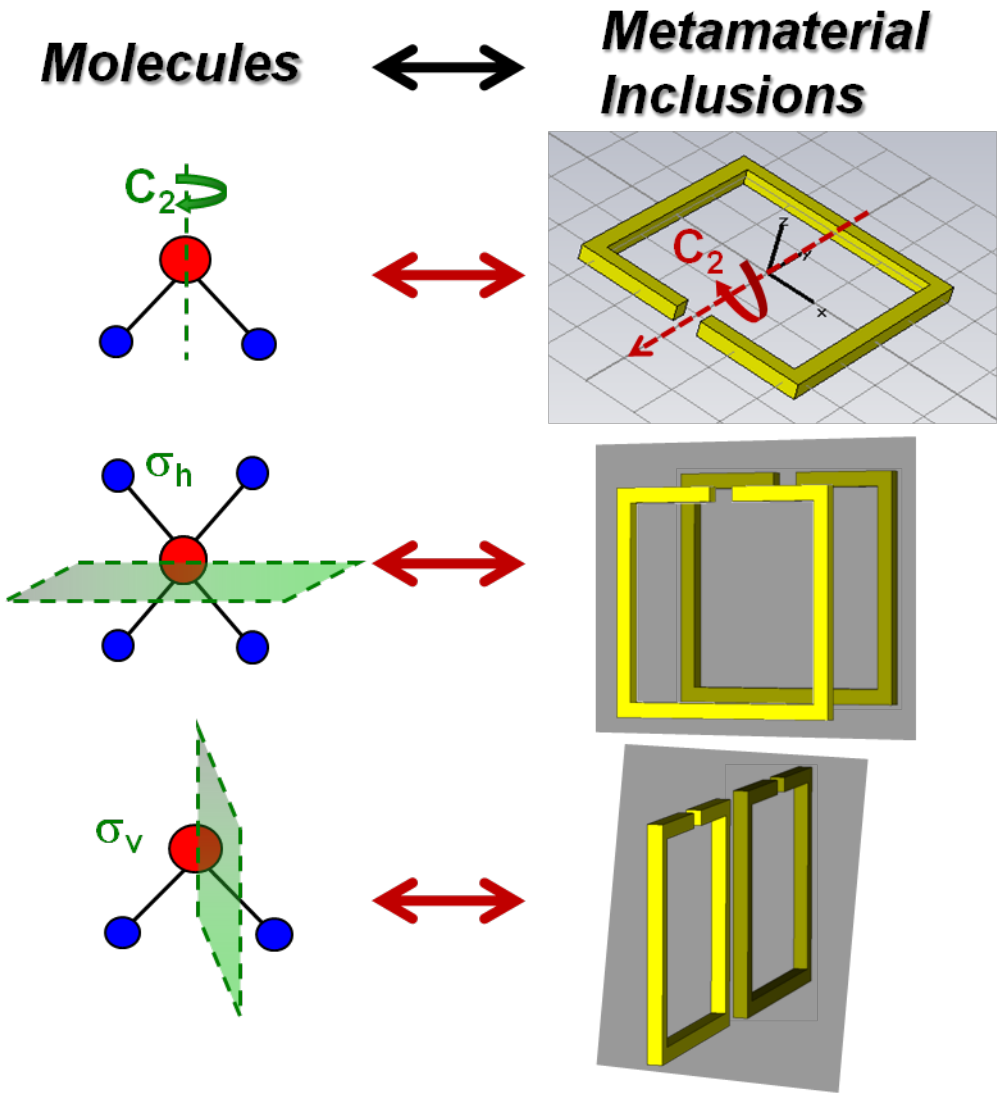

Figure 1.

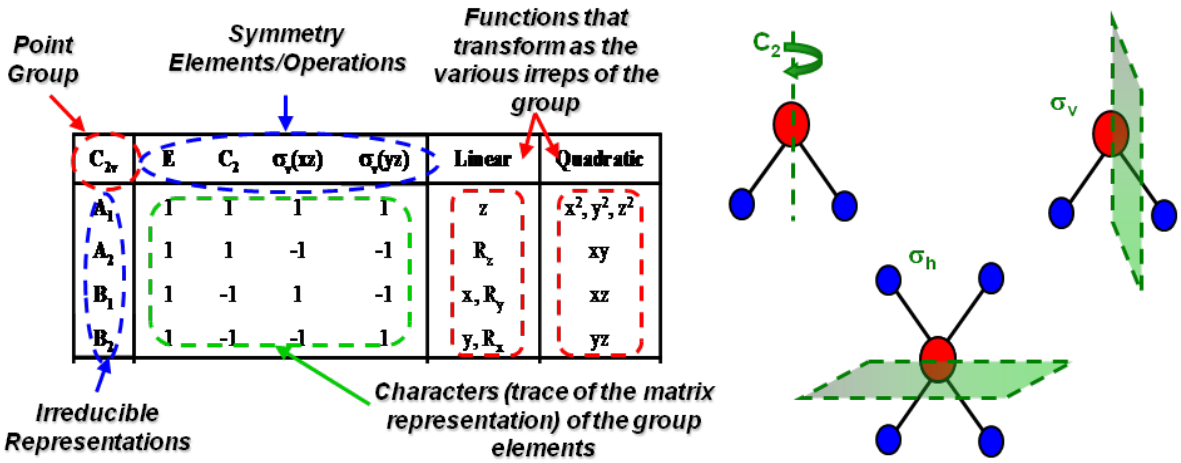
Point Group
Symmetry Elements/Operations
Functions that transform as the various irreps of the group
C2v
E
C2
σv(xz)
σv(yz)
Linear
Quadratic
A1 1 1 1 1 z x2, y2, z2
A2 1 1 -1 -1 Rz xy
B1 1 -1 1 -1 x, Ry xz
B2 1 -1 -1 1 y, Rx yz
Irreducible Representations
Characters (trace of the matrix representation) of the group elements
C2
σv
σh

Figure 2.

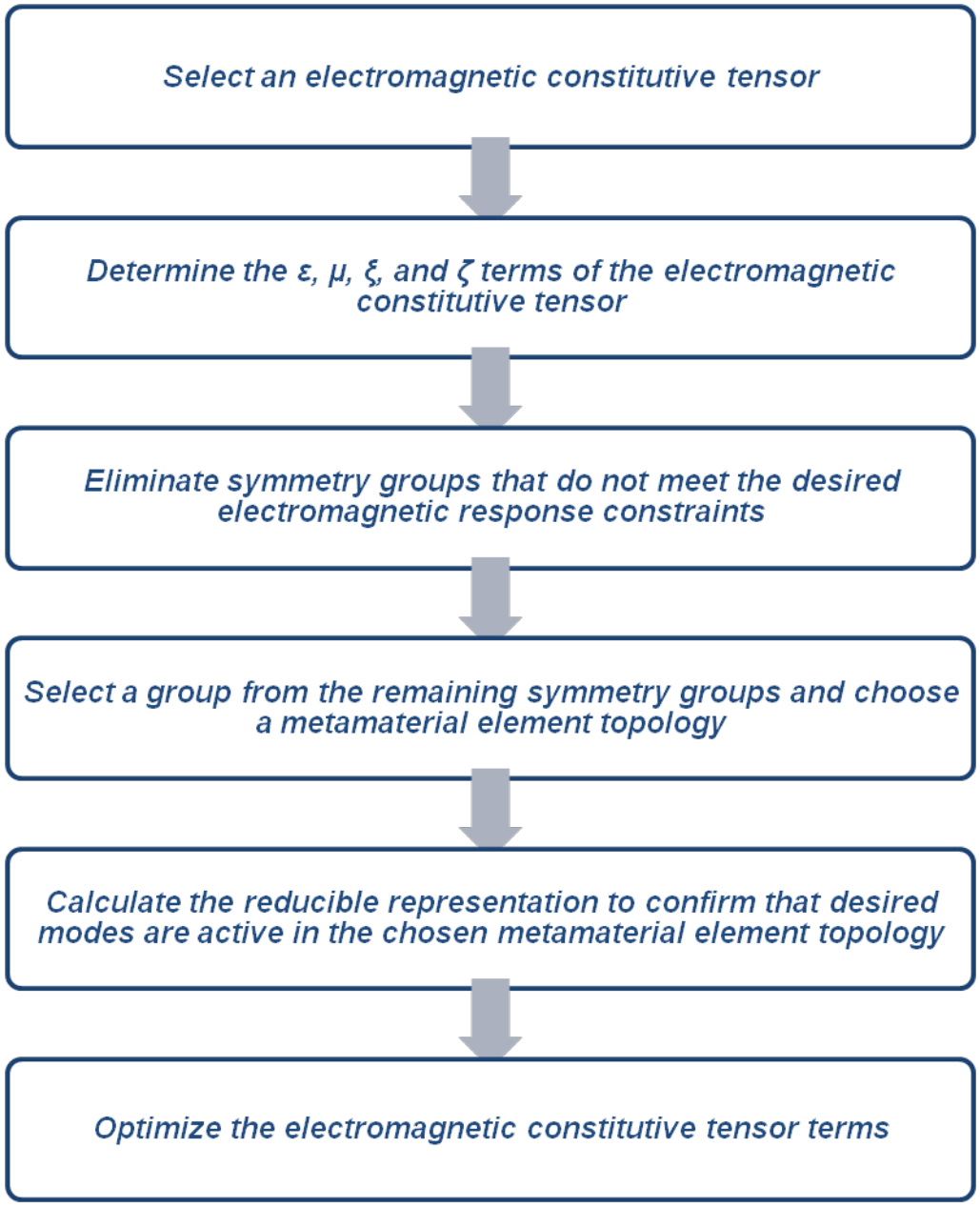
Select an electromagnetic constitutive tensor
Determine the ε, μ, ξ, and ζ terms of the electromagnetic constitutive tensor
Eliminate symmetry groups that do not meet the desired electromagnetic response constraints
Select a group from the remaining symmetry groups and choose a metamaterial element topology
Calculate the reducible representation to confirm that desired modes are active in the chosen metamaterial element topology
Optimize the electromagnetic constitutive tensor terms

Figure 3.

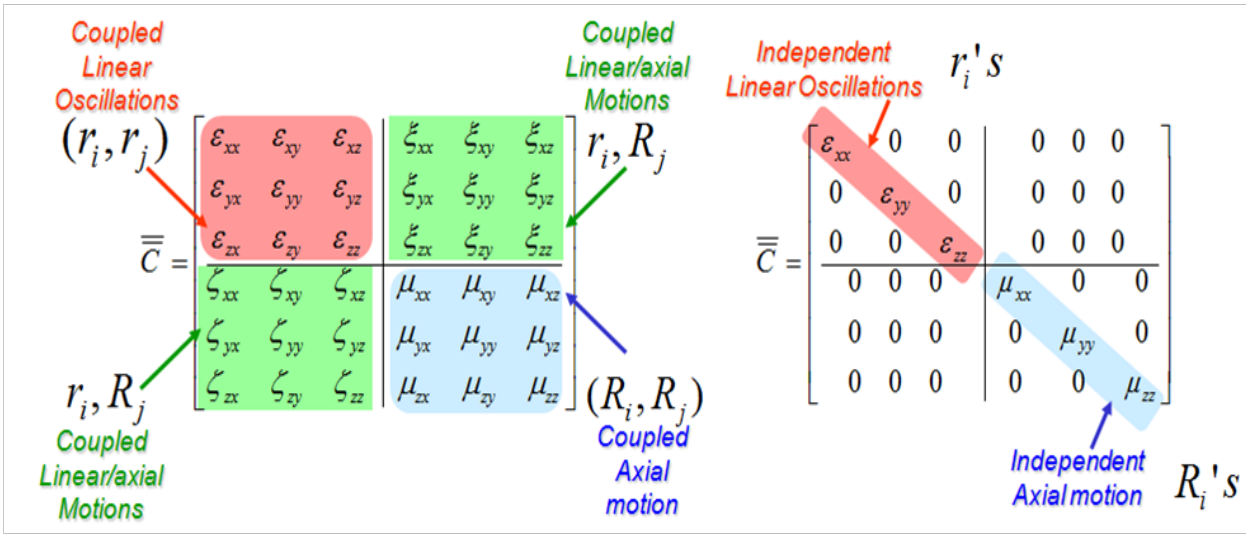
Coupled Linear Oscillations
(r_i, r_j)
Coupled Linear/axial Motions
r_i, R_j
$\overline{\overline{C}} =$
r_i, R_j
Coupled Linear/axial Motions
(R_i, R_j)
Coupled Axial motion
Independent Linear Oscillations
$r_i's$
$\overline{\overline{C}} =$
Independent Axial motion
$R_i's$

Figure 4.

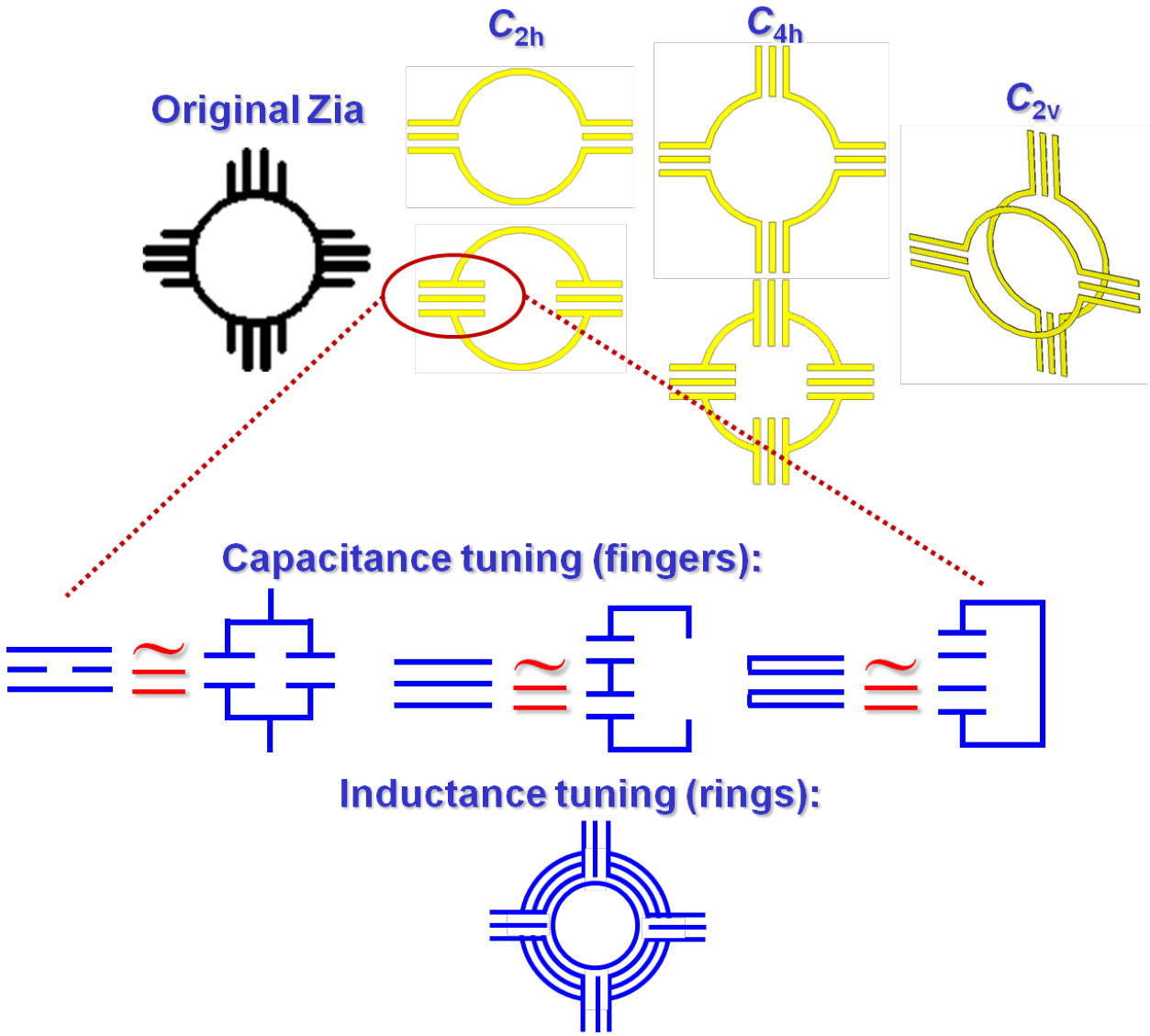
Original Zia
C2h
C4h
C2v
Capacitance tuning (fingers):
Inductance tuning (rings):

Figure 5.

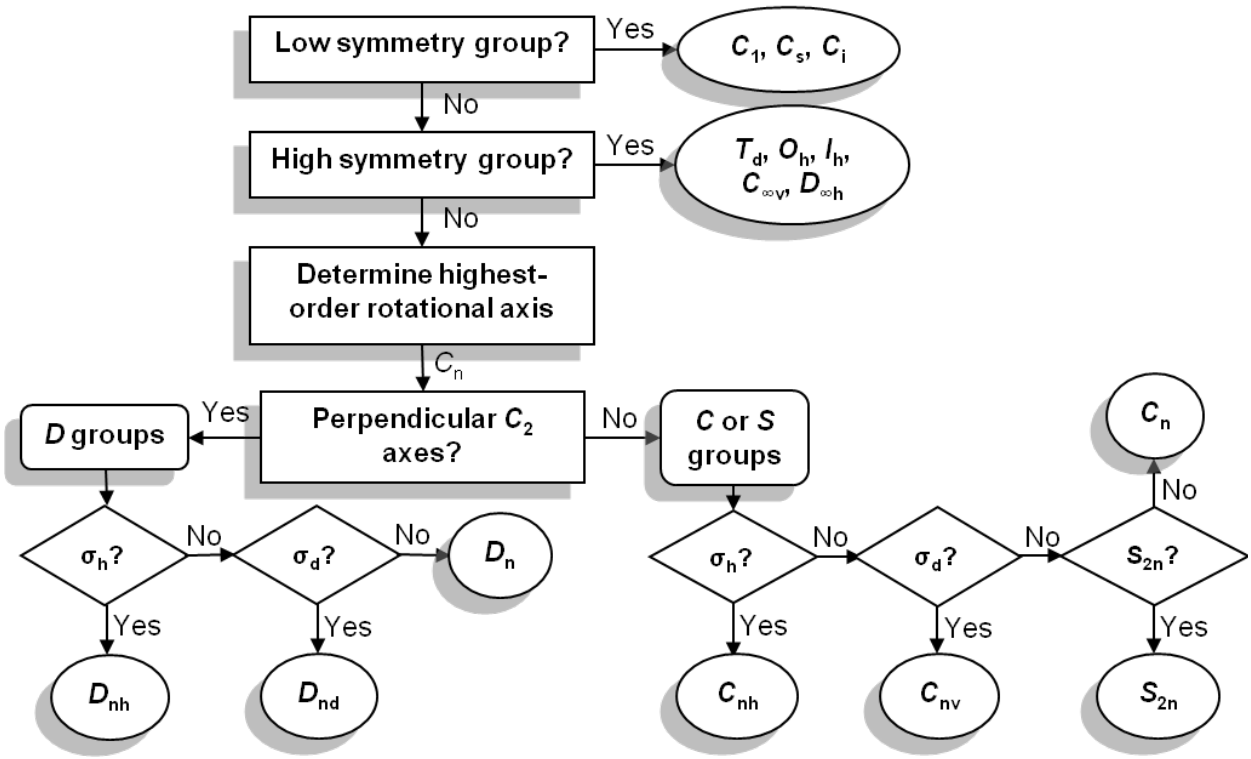
Low symmetry group?
Yes
C_1, C_s, C_i
No
High symmetry group?
Yes
T_d, O_h, I_h, $C_{\infty v}$, $D_{\infty h}$
No
Determine highest-order rotational axis
C_n
Perpendicular C_2 axes?
Yes
D groups
No
C or S groups
σ_h?
No
σ_d?
No
D_n
Yes
D_{nh}
Yes
D_{nd}
σ_h?
No
σ_d?
No
S_{2n}?
No
C_n
Yes
C_{nh}
Yes
C_{nv}
Yes
S_{2n}

Figure 6.

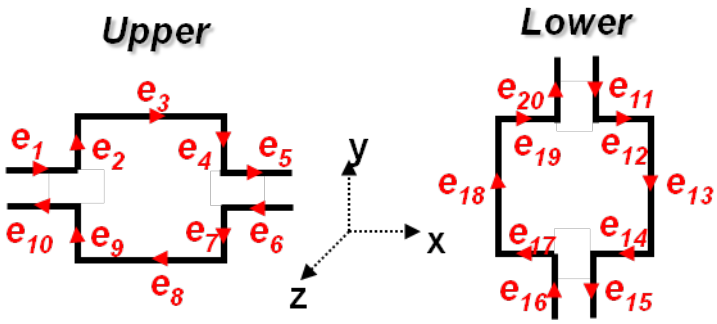
Upper
Lower
e1
e2
e3
e4
e5
e6
e7
e8
e9
e10
e11
e12
e13
e14
e15
e16
e17
e18
e19
e20
y
x
z
Figure 7.

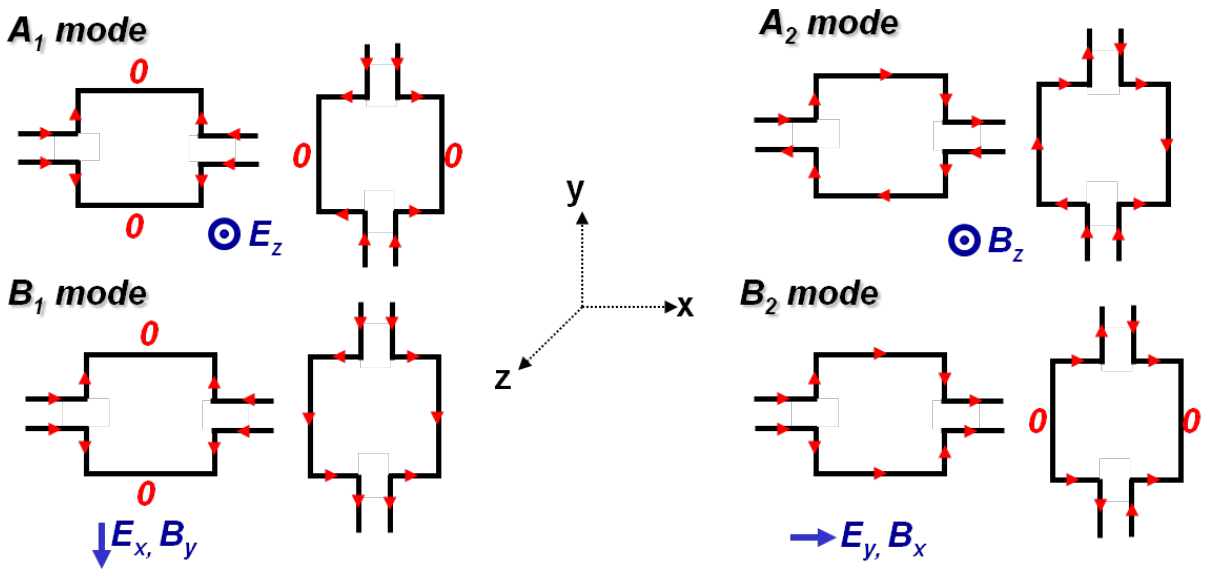

Figure 8.

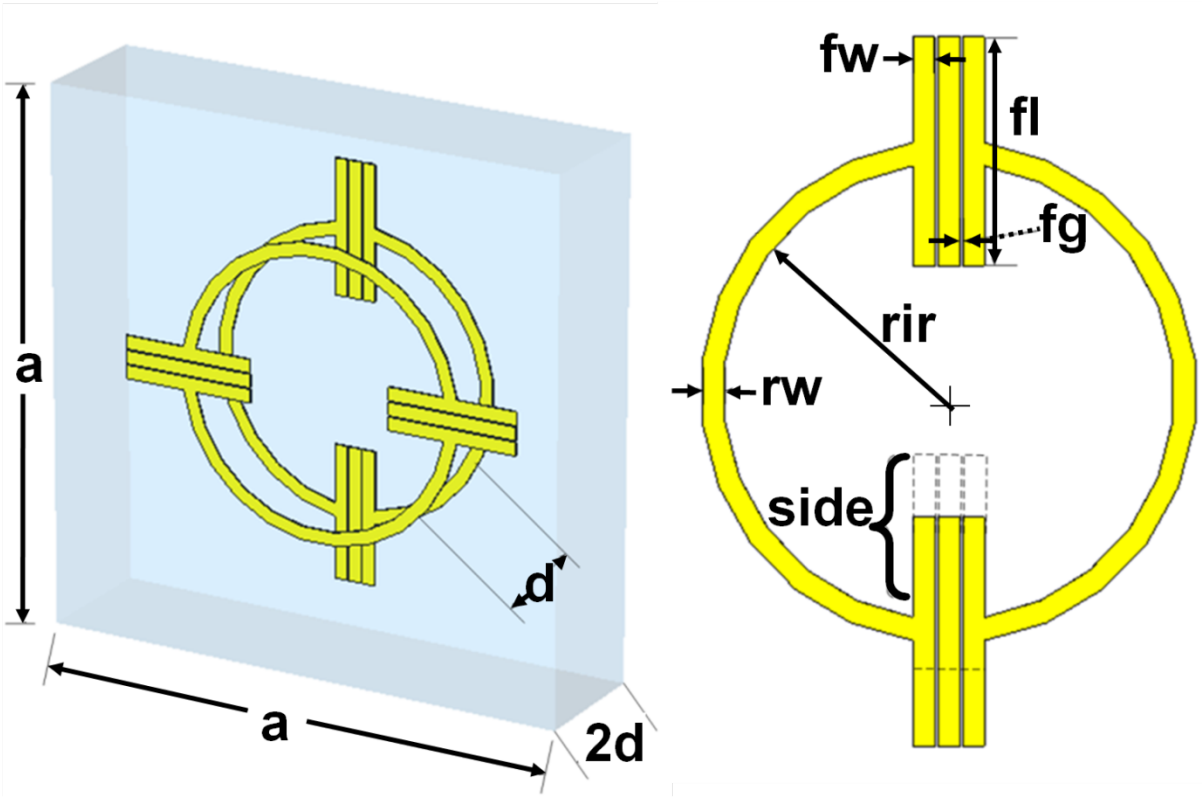

Figure 9.

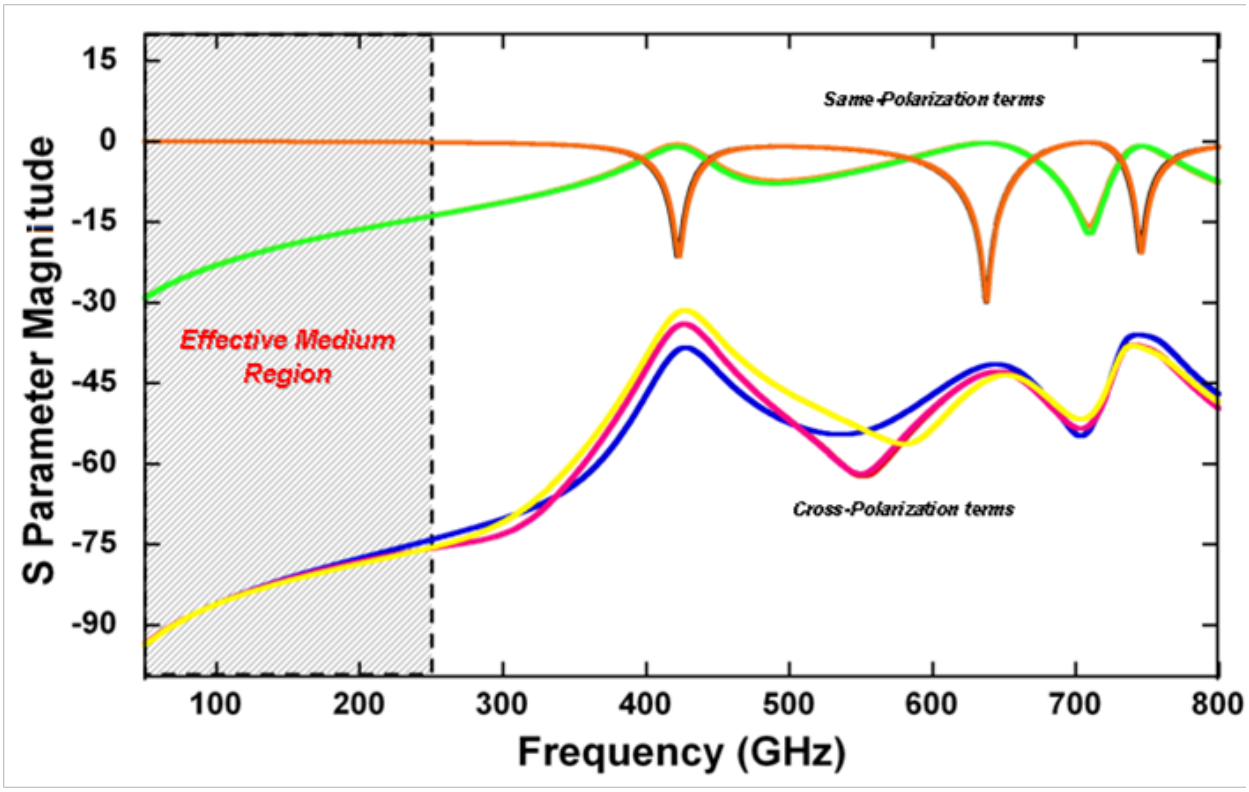
15
0
-15
-30
-45
-60
-75
-90
S Parameter Magnitude
100
200
300
400
500
600
700
800
Frequency (GHz)
Same-Polarization terms
Cross-Polarization terms
Effective Medium
Region
Figure 10.

Figure 11.

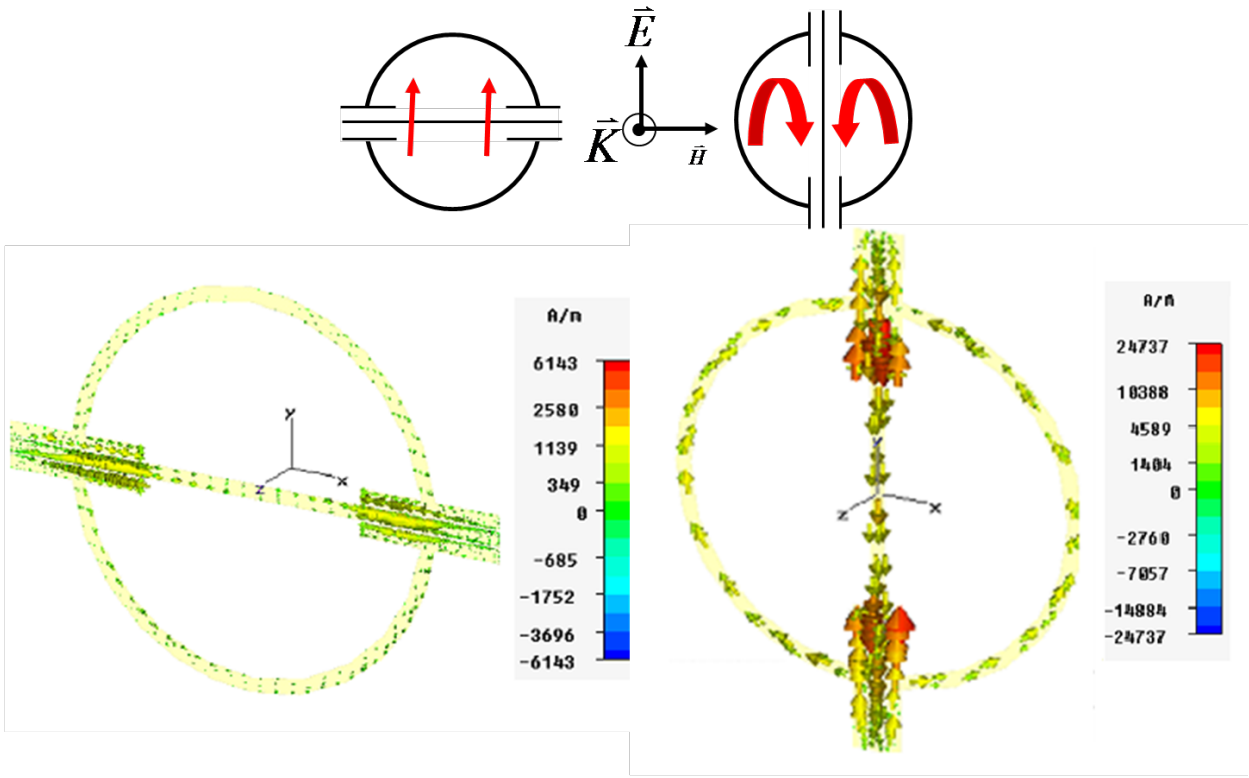
$\vec{E}$
$\vec{K}$
$\vec{H}$
A/m
6143
2580
1139
349
0
-685
-1752
-3696
-6143
A/m
24737
10388
4589
1404
0
-2760
-7057
-14884
-24737

Figure 12.

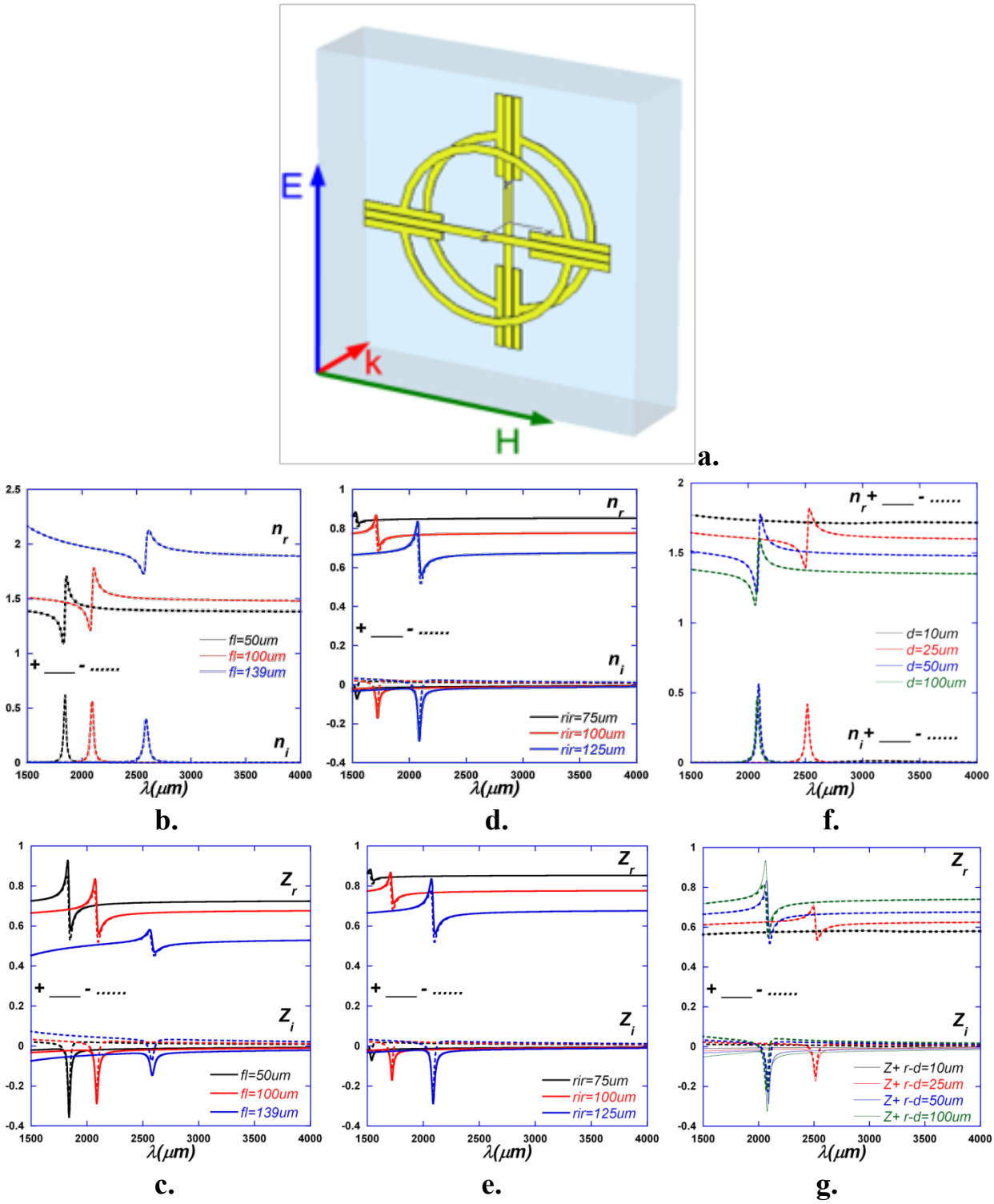
E
k
H
a.
n_r
n_i
fl=50um
fl=100um
fl=139um
b.
rir=75um
rir=100um
rir=125um
d.
d=10um
d=25um
d=50um
d=100um
f.
Z_r
Z_i
c.
e.
Z+ r-d=10um
Z+ r-d=25um
Z+ r-d=50um
Z+ r-d=100um
g.
λ(μm)

Figure 13.

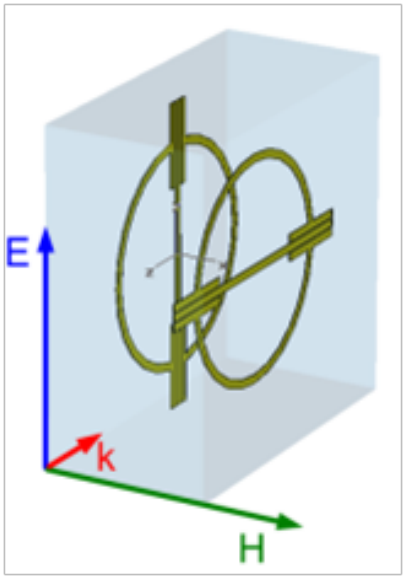

a.

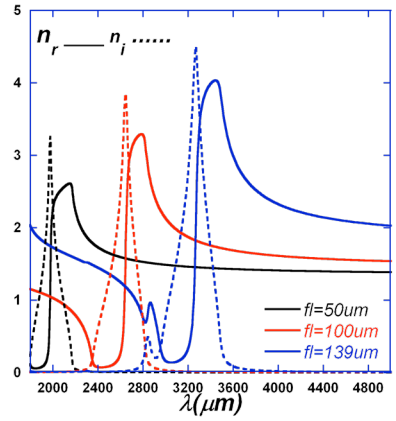

b.

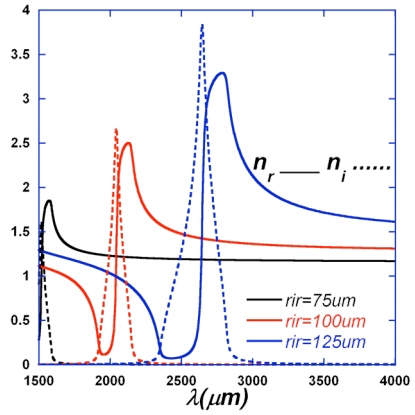

d.

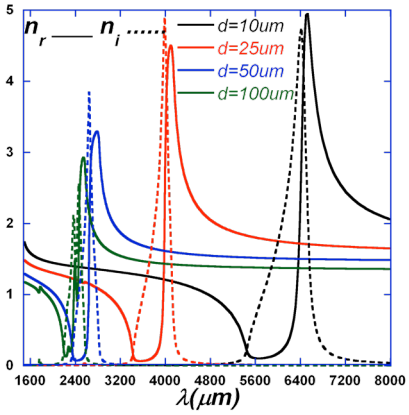

f.

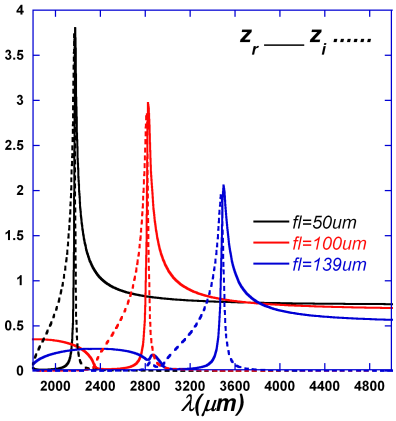

c.

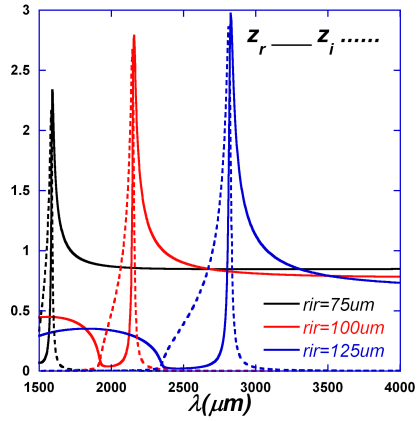

e.

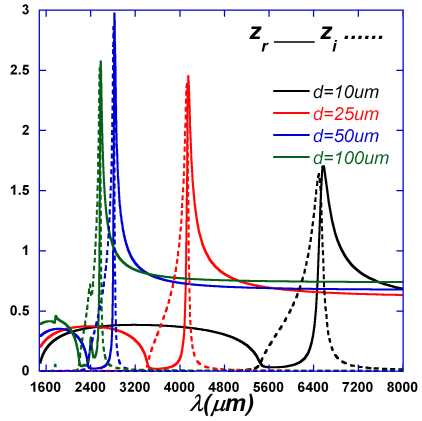

g.

Figure 14.

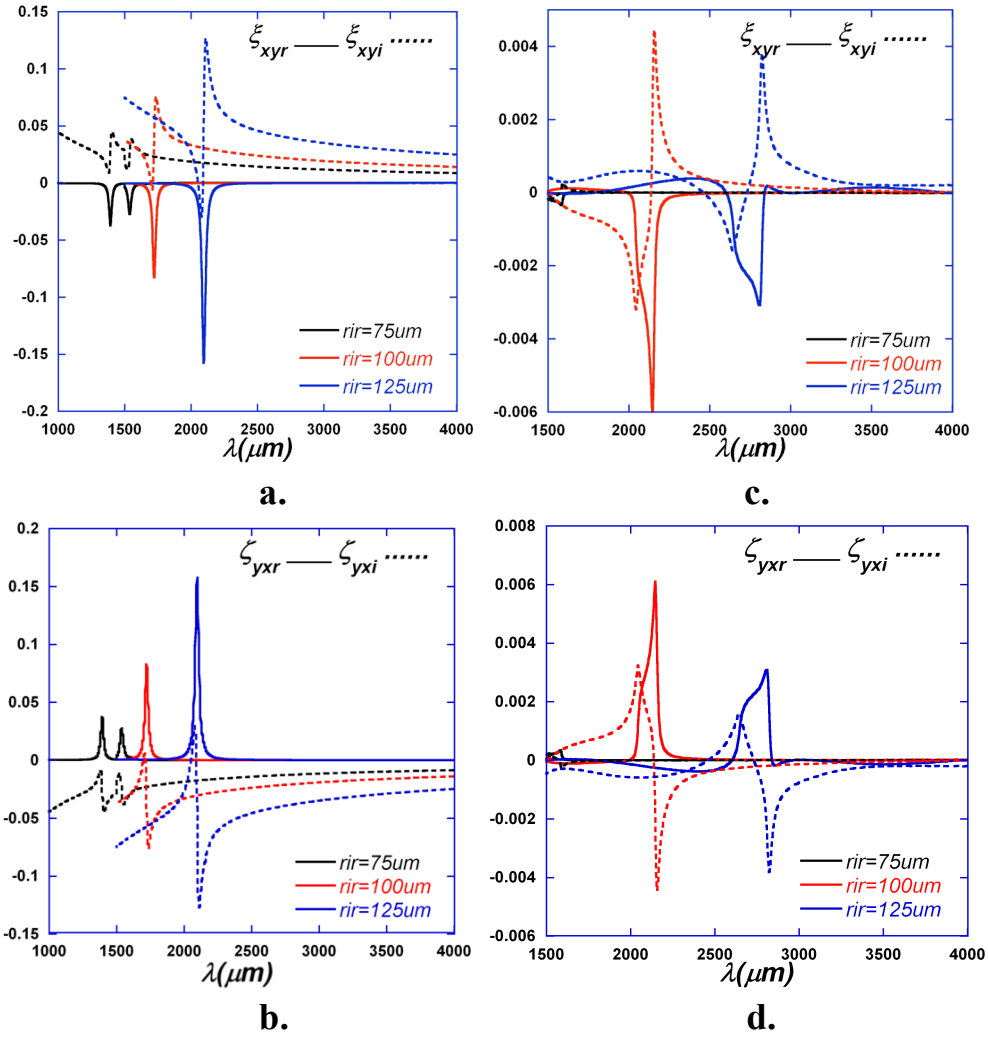
ξ_{xyr} —— ξ_{xyi} ……
rir=75um
rir=100um
rir=125um
λ(μm)
a.
c.
ζ_{yxr} —— ζ_{yxi} ……
b.
d.

Figure 15.

$\mathbf{D_2}$	E	C_2 (z)	C_2 (y)	C_2 (x)	linear functions, rotations
A	+1	+1	+1	+1	-
B_1	+1	+1	-1	-1	z, R_z
B_2	+1	-1	+1	-1	y, R_y
B_3	+1	-1	-1	+1	x, R_x

a.

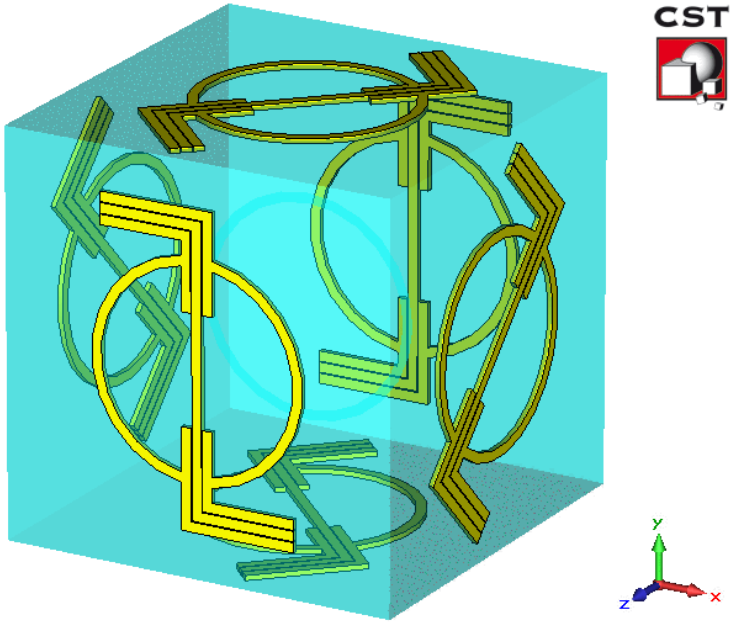

b.

Figure 16.

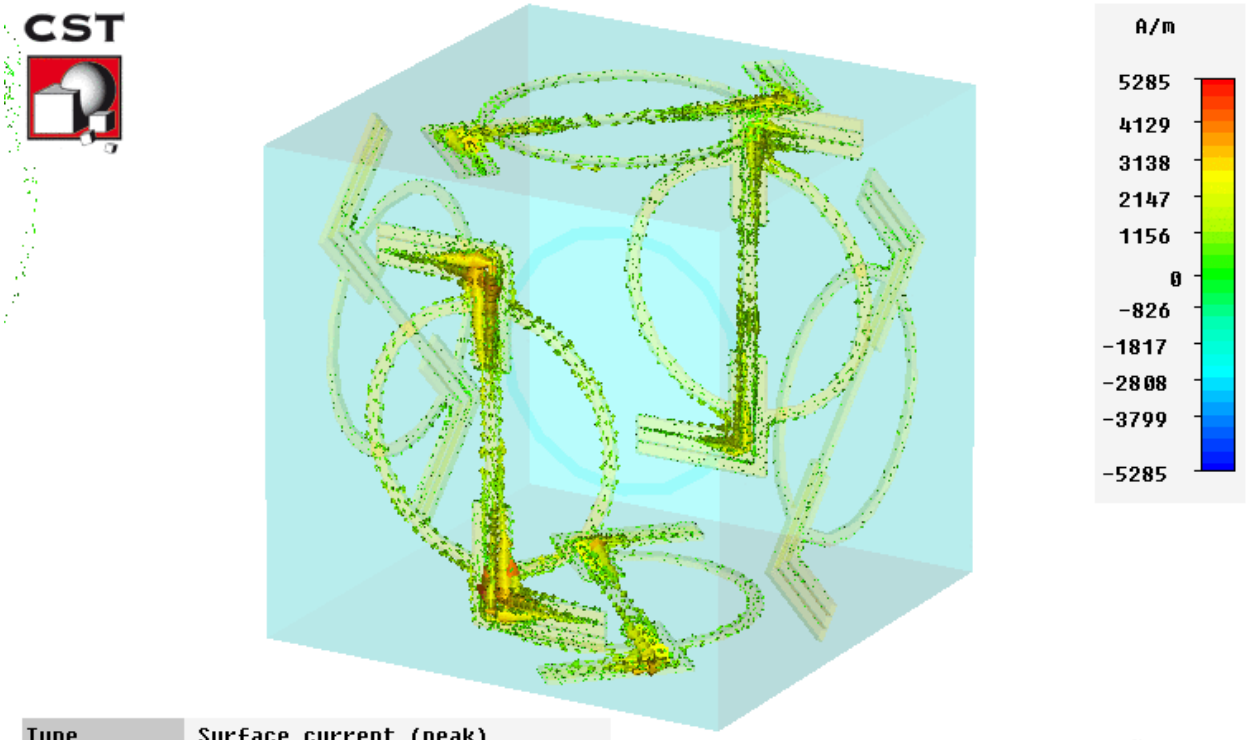
CST
A/m
5285
4129
3138
2147
1156
0
-826
-1817
-2808
-3799
-5285
Type Surface current (peak)
Monitor h-field (f=187.36)
Maximum-3D 6646.95 A/m at 5 / -98.88 / 195
Frequency 187.36
Phi 0 degrees
Theta 0 degrees
Phase 0 degrees
y
z
x

Figure 17.

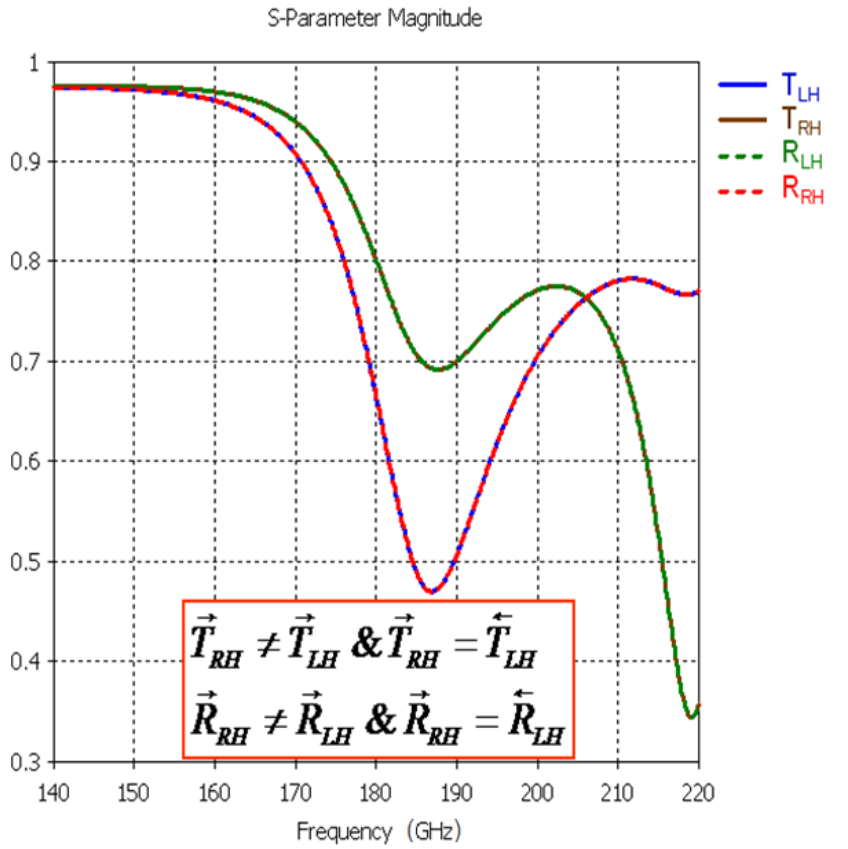
S-Parameter Magnitude
1
0.9
0.8
0.7
0.6
0.5
0.4
0.3
140
150
160
170
180
190
200
210
220
Frequency (GHz)
T_LH
T_RH
R_LH
R_RH
$\vec{T}_{RH} \neq \vec{T}_{LH} \;\&\; \vec{T}_{RH} = \overleftarrow{T}_{LH}$
$\vec{R}_{RH} \neq \vec{R}_{LH} \;\&\; \vec{R}_{RH} = \overleftarrow{R}_{LH}$

a.

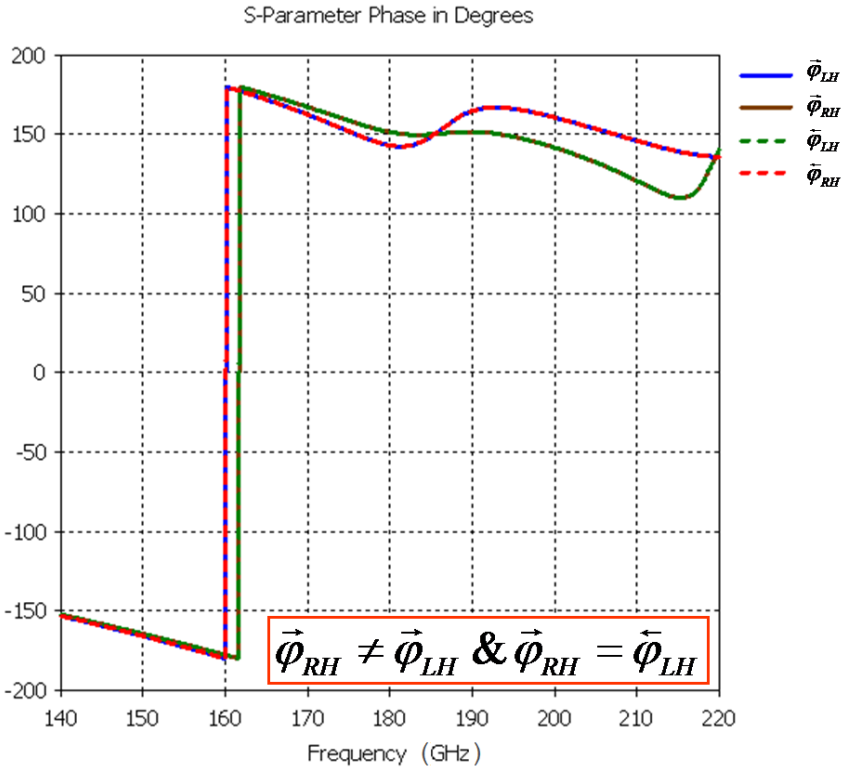
S-Parameter Phase in Degrees
200
150
100
50
0
-50
-100
-150
-200
140
150
160
170
180
190
200
210
220
Frequency (GHz)
$\vec{\varphi}_{LH}$
$\vec{\varphi}_{RH}$
$\overleftarrow{\varphi}_{LH}$
$\overleftarrow{\varphi}_{RH}$
$\vec{\varphi}_{RH} \neq \vec{\varphi}_{LH} \;\&\; \vec{\varphi}_{RH} = \overleftarrow{\varphi}_{LH}$

b.

Figure 18.

D_{2h}	E	C_2 (z)	C_2 (y)	C_2 (x)	i	σ (xy)	σ (xz)	σ (yz)	linear functions, rotations
A_g	+1	+1	+1	+1	+1	+1	+1	+1	-
B_{1g}	+1	+1	-1	-1	+1	+1	-1	-1	R_z
B_{2g}	+1	-1	+1	-1	+1	-1	+1	-1	R_y
B_{3g}	+1	-1	-1	+1	+1	-1	-1	+1	R_x
A_u	+1	+1	+1	+1	-1	-1	-1	-1	-
B_{1u}	+1	+1	-1	-1	-1	-1	+1	+1	z
B_{2u}	+1	-1	+1	-1	-1	+1	-1	+1	y
B_{3u}	+1	-1	-1	+1	-1	+1	+1	-1	x

a.

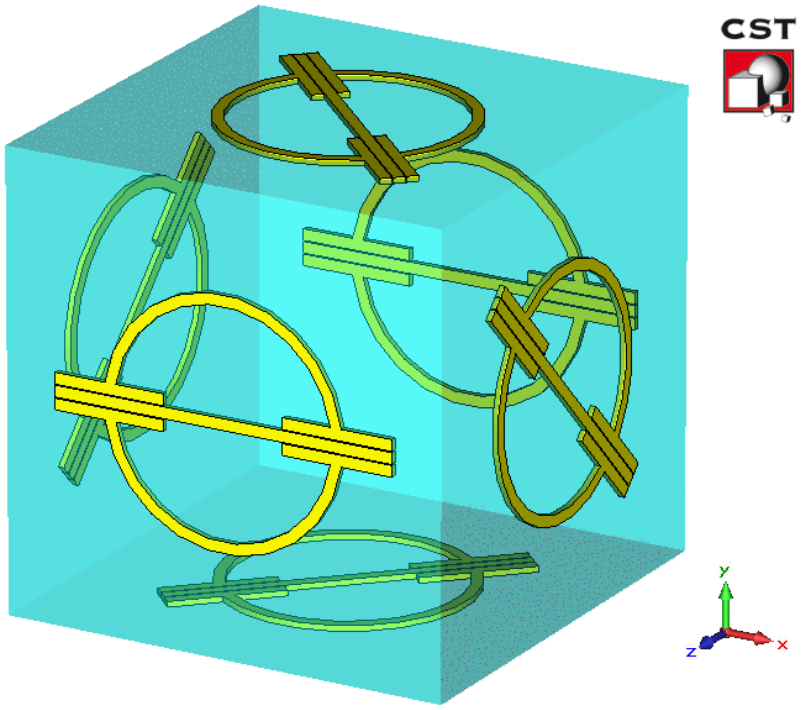

b.

Figure 19.

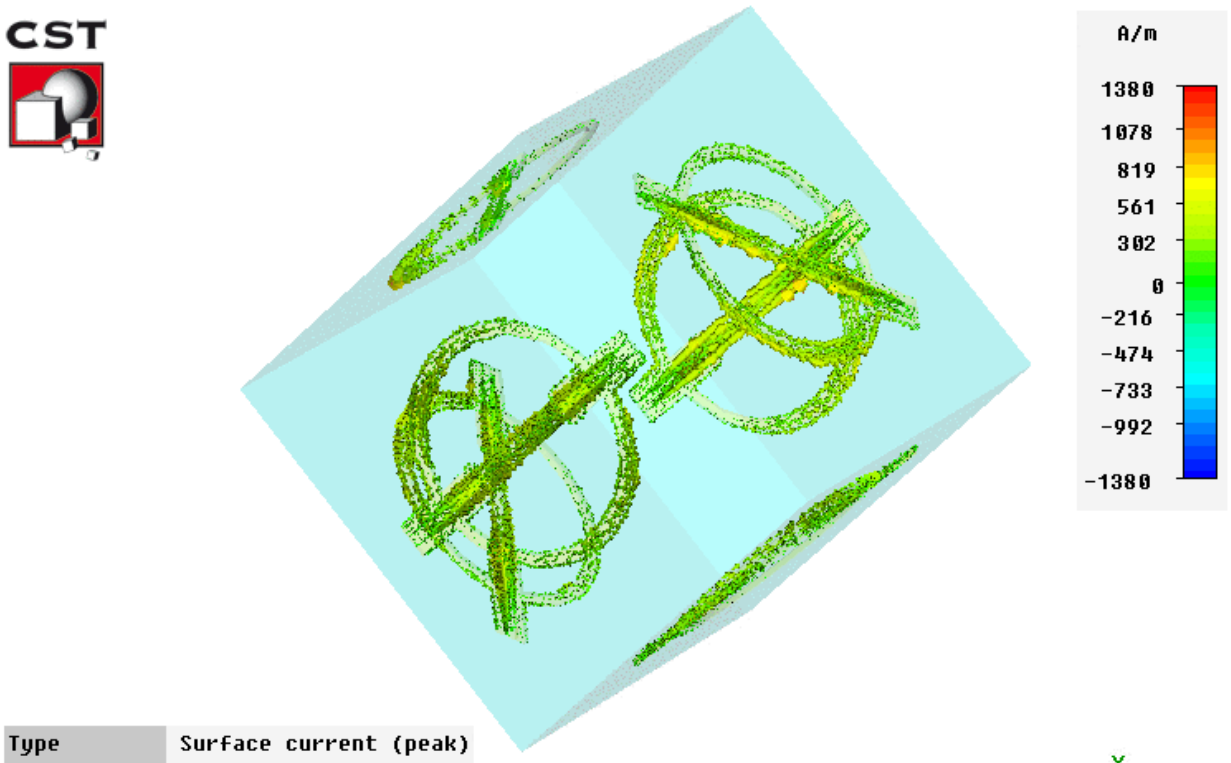

Type	Surface current (peak)
Monitor	h-field (f=220)
Maximum-3D	2161.46 A/m at 93.0327 / -182.739 / 70.503
Frequency	220
Phi	0 degrees
Theta	0 degrees
Phase	0 degrees

Figure 20.

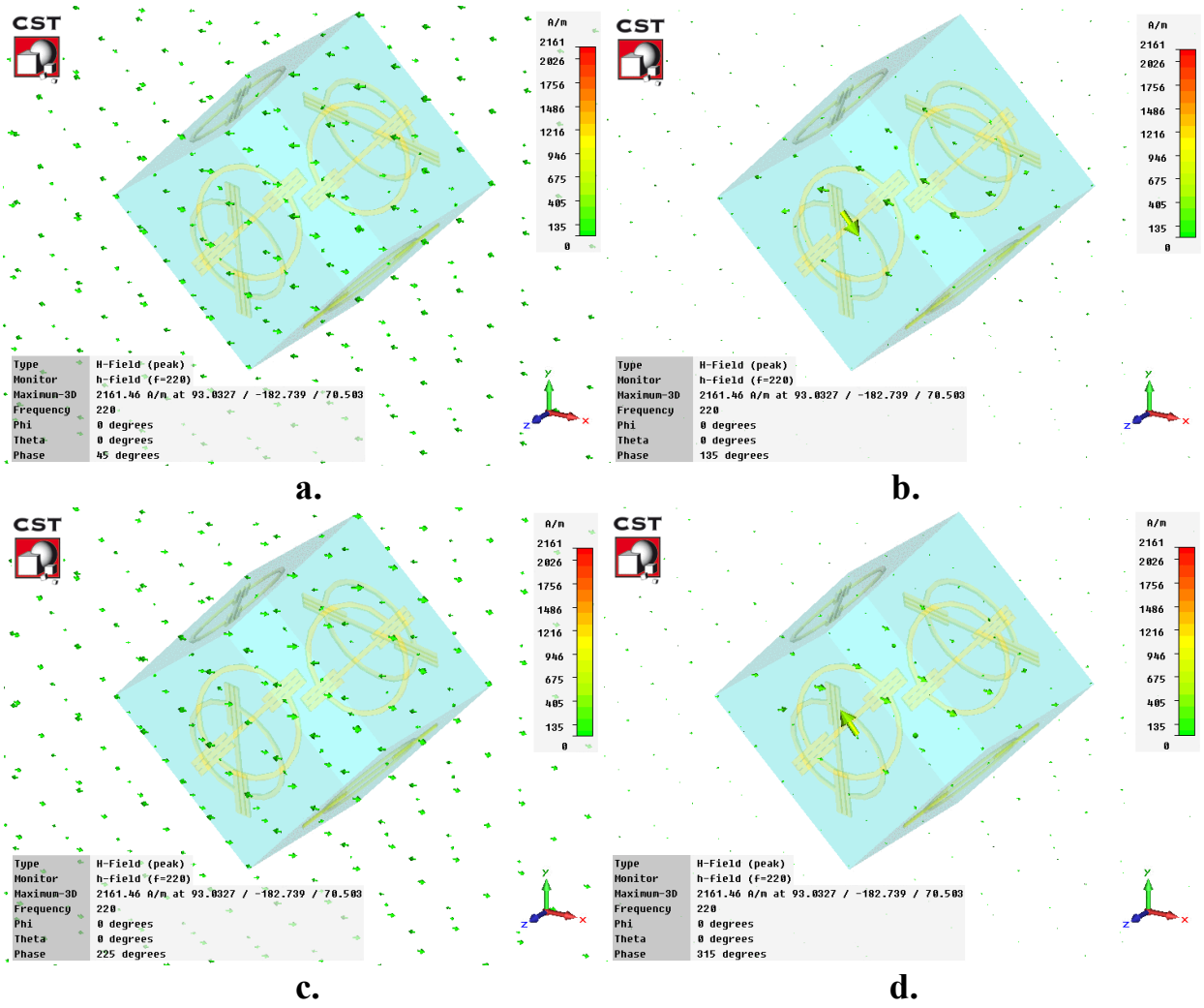
CST
A/m
2161
2026
1756
1486
1216
946
675
405
135
0
Type H-Field (peak)
Monitor h-field (f=220)
Maximum-3D 2161.46 A/m at 93.0327 / -182.739 / 70.503
Frequency 220
Phi 0 degrees
Theta 0 degrees
Phase 45 degrees
a.
Type H-Field (peak)
Monitor h-field (f=220)
Maximum-3D 2161.46 A/m at 93.0327 / -182.739 / 70.503
Frequency 220
Phi 0 degrees
Theta 0 degrees
Phase 135 degrees
b.
Type H-Field (peak)
Monitor h-field (f=220)
Maximum-3D 2161.46 A/m at 93.0327 / -182.739 / 70.503
Frequency 220
Phi 0 degrees
Theta 0 degrees
Phase 225 degrees
c.
Type H-Field (peak)
Monitor h-field (f=220)
Maximum-3D 2161.46 A/m at 93.0327 / -182.739 / 70.503
Frequency 220
Phi 0 degrees
Theta 0 degrees
Phase 315 degrees
d.

Figure 21.

LIST OF TABLES

Table 1. List of symmetry groups and their corresponding electromagnetic behaviors subject to the activity of the designated modes.

Group	**Active Modes**	**Behavior**
C_1	A	unspecified
C_s	A', A''	general bianisotropic
C_i	A_g, A_u	biaxial
C_2	A B	chiral bianisotropic
C_3	A E	chiral general bianisotropic
C_4	A B E	chiral unspecified general bianisotropic
C_5	A E_1 E_2	chiral general bianisotropic unspecified
C_6	A B, E_2 E_1	chiral unspecified general bianisotropic
C_7	A E_1 E_2, E_3	chiral general bianisotropic unspecified
C_8	A B, E_2, E_3 E_1	chiral unspecified general bianisotropic
C_{2v}	A_1, A_2 B_1, B_2	uniaxial bianisotropic
C_{3v}	A_1, A_2 E	uniaxial general bianisotropic
C_{4v}	A_1, A_2 B_1, B_2	uniaxial unspecified

	E	general bianisotropic
C_{5v}	A_1, A_2 E_1 E_2	uniaxial general bianisotropic unspecified
C_{6v}	A_1, A_2 B_1, B_2, E_2 E_1	uniaxial unspecified general bianisotropic
C_{2h}	A_g, A_u B_g, B_u	uniaxial biaxial
C_{3h}	A’, A’’ E’, E’’	uniaxial general anisotropic
C_{4h}	A_g, A_u B_g, B_u E_g, E_u	uniaxial unspecified general anisotropic
C_{5h}	A’, A’’ E_1’, E_1’’ E_2’, E_2’’	uniaxial general anisotropic unspecified
C_{6h}	A_g, A_u B_g, B_u, E_{2g}, E_{2u} E_{1g}, E_{1u}	uniaxial unspecified general anisotropic
D_2	A B_1, B_2, B_3	unspecified chiral
D_3	A_1 A_2 E	unspecified chiral general bianisotropic
D_4	A_1, B_1, B_2 A_2 E	unspecified chiral general bianisotropic
D_5	A_1, E_2 A_2 E_1	unspecified chiral general bianisotropic
D_6	A_1, B_1, B_2, E_1 A_2 E_2	unspecified chiral general bianisotropic
D_{2d}	A_1, B_1 A_2, B_2 E	unspecified uniaxial general bianisotropic

D_{3d}	A_{1g}, A_{1u} A_{2g}, A_{2u} E_g, E_u	unspecified uniaxial general anisotropic
D_{4d}	A_1, B_1, E_2 A_2, B_2 E_1, E_3	unspecified uniaxial general bianisotropic
D_{5d}	A_{1g}, E_{2g}, A_{1u}, E_{2u} A_{2g}, A_{2u} E_{1g}, E_{1u}	unspecified uniaxial general anisotropic
D_{6d}	A_1, B_1, E_2, E_3, E_4 A_2, B_2 E_1, E_5	unspecified uniaxial general bianisotropic
D_{2h}	A_g, A_u B_{1g}, B_{2g}, B_{3g}, B_{1u}, B_{2u}, B_{3u}	unspecified uniaxial, biaxial
D_{3h}	A_1', A_1'' A_2', A_2'' E', E''	unspecified uniaxial general anisotropic
D_{4h}	A_{1g}, B_{1g}, B_{2g}, A_{1u}, B_{1u}, B_{2u} A_{2g}, A_{2u} E_g, E_u	unspecified uniaxial general anisotropic
D_{5h}	A_1', A_1'', E_1', E_1'' A_2', A_2'' E_1', E_1''	unspecified uniaxial general anisotropic
D_{6h}	A_{1g}, B_{1g}, B_{2g}, E_{2g}, A_{1u}, B_{1u}, B_{2u}, E_{2u} A_{2g}, A_{2u} E_{1g}, E_{1u}	unspecified uniaxial general anisotropic
D_{8h}	A_{1g}, B_{1g}, B_{2g}, E_{2g}, E_{3g}, A_{1u}, B_{1u}, B_{2u}, E_{2u}, E_{3u} A_{2g}, A_{2u} E_{1g}, E_{1u}	unspecified uniaxial general anisotropic
$C_{\infty v}$	A_1, A_2 E_1 E_2, $E_{3,}$ …	uniaxial bianisotropic unspecified
$D_{\infty h}$	A_{1g}, E_{2g}, A_{2u}, $E_{2u,}$ …	unspecified

	A_{2g}, A_{1u} E_{1g}, E_{1u}	 uniaxial general anisotropic
S_4	A, B E	uniaxial bianisotropic
S_6	A_g, A_u E_g, E_u	uniaxial general anisotropic
S_8	A, B E_1 E_2, E_3	uniaxial bianisotropic unspecified
T	A, E T	unspecified general bianisotropic
T_d	A_1, A_2, E T_1, T_2	unspecified general anisotropic
T_h	A_g, A_u, E_g, E_u T_g, T_u	unspecified general anisotropic
O	A_1, A_2, E, T_2 T_1	unspecified general bianisotropic
O_h	A_{1g}, A_{2g}, E_g, T_{2g}, A_{1u}, A_{2u}, E_u, T_{2u} T_{1g}, T_{1u}	unspecified general anisotropic
I	A, T_2, G, H T_1	unspecified general bianisotropic
I_h	A_g, T_{2g}, G_g, H_g, A_u, T_{2u}, G_g, H_g T_{1g}, T_{1u}	unspecified general anisotropic